

# CHALMERS



## Modelling of Pneumatic Engine I

Master's Thesis in the Master's programme in Sound and Vibration

AMÉLIE RENAULT



**TRELLEBORG**  
AUTOMOTIVE

Department of Civil and Environmental Engineering  
*Division of Division of Applied Acoustics*  
*Vibroacoustics Group*  
CHALMERS UNIVERSITY OF TECHNOLOGY  
Göteborg, Sweden 2005

Master's Thesis 2005:48

MASTER'S THESIS 2005:48

# Modelling of Pneumatic Engine Mount

AMÉLIE RENAULT

Supervisors:

Lars H. Ivarsson (Department of Applied Acoustics)  
Arndt Graeve (Trelleborg Automotive)

Department of Civil and Environmental Engineering  
Division of Applied Acoustics  
Vibroacoustics Group  
CHALMERS UNIVERSITY OF TECHNOLOGY  
Göteborg, Sweden 2005

TRELLEBORG Automotive

Modelling of Pneumatic Engine Mount

© AMÉLIE RENAULT, 2005

Master's Thesis 2005:48

Department of Civil and Environmental Engineering  
Division of Applied Acoustics  
Vibroacoustics Group  
Chalmers University of Technology  
SE-41296 Göteborg  
Sweden

Telephone +46 (0)31-772 1000

Reproservice / Department of Civil and Environmental Engineering  
Göteborg, Sweden 2005

Modelling of Pneumatic Engine Mount  
AMÉLIE RENAULT  
Department of Civil and Environmental Engineering  
Division of Applied Acoustics  
Vibroacoustics Group  
Chalmers University of Technology

## Abstract

The goal of this Master thesis has been to build a mathematical model of a pneumatic damped engine mount, which could be a cost effective alternative to hydraulically damped engine mount. This model will help to understand the pneumatic mount and its damping mechanism.

An engine mount must satisfy at least two essential but conflicting criteria.

First, the mount has to carry the static gravity load of the engine.

The second requirement is that the compartment should be isolated from vibrations and acoustically comfortable: the mount has to be compliant and lightly damped for small excitation amplitudes and over the higher frequency range.

The third requirement is to isolate the car from the motions due to bumpy roads, abrupt vehicle acceleration or deceleration, and braking and cornering. That means that the mount has to be stiff and highly damped

Conventional rubber mount cannot satisfy both requirements simultaneously and a compromise between resonance control and isolation is inevitably needed, which is to get non-linear stiffness and damping dependant on frequency. There are many disadvantages to the hydro mounts: it is big, heavy, complicated and expensive.

Then, an air damped engine mount could be an issue to decrease the size of the damping device (it has only one chamber) and lower the price (it is quite simple and is based on air compression). But a pneumatic mount is less damped than the hydro mount and the damping has to be increased in order to damp heavy engines. In this report will be presented an overview about hydro-mechanical mount, pneumatic mounts and some tools that will be used to model the rubber dynamic properties, the air volume and the orifice behavior. After that, the model will be explained. Finally, some proposals how to increase the damping will be explained.

After having understood how an hydraulic mount is working and explored some simple pneumatic spring, the model of the pneumatic mount has been implemented in MATLAB and finally, the calculated curves are compared to the measured one. The mount has physically been divided in three parts in order to model it more easily and the conclusion of the model-experiment study shows that:

- The rubber part is well modelled with a spring in parallel with a dashpot,
- The orifice impedances seems to be quite correctly modelled since the global model predicts really well the resonance frequency
- The air compliance is not modelled accurately enough.

It can be also remarked that the simplified orifice impedance is working well for the chosen frequency range and for this application.

**Keywords:** Engine mount, pneumatic mount, damping modelling, orifice damping, engine suspension.



## **Acknowledgments**

It was really great to do my master thesis at the acoustic department. I would like to thank Lars Ivarsson for being a patient and good supervisor, Wolfgang for helping me with the physical understanding of my subject, Börje for fixing my different computer problems and of course also Gunilla for all administrative things.

Thanks to all my friends for the great time, which allowed me to spend a less boring thesis. I will never forget the balcony discussions and the 'fika' time which allow to take energy and forget the stress...

To my little sister who waited such a long time for me to come back home.

# I. Introduction

The goal of this Master thesis is to build a mathematical model of a pneumatic damped engine mount, which could be a cheap alternative to hydraulically damped engine mount. This model will help to understand the pneumatic mount and its damping mechanism.

An engine mount must satisfy at least two essential but conflicting criteria.

First, the mount has to carry the static gravity load of the engine.

The second requirement is that the compartment should be isolated from vibrations and acoustically comfortable: the mount has to be compliant and lightly damped for small excitation amplitudes and over the higher frequency range.

The third requirement is to isolate the car from the motions due to bumpy roads, abrupt vehicle acceleration or deceleration, and braking and cornering. That means that the mount has to be stiff and highly damped

Conventional rubber mount cannot satisfy both requirements simultaneously as the lumped stiffness,  $k_r$ , and the viscous damping coefficient,  $b_r$ , in the shear mode are nearly invariant with excitation amplitude and frequency over the concerned excitation range of vehicle systems. Thus, a compromise between resonance control and isolation is inevitably needed, which is to get non-linear stiffness and damping dependant on frequency. The hydro mount is typically optimized for placement, orientation,  $k_r$  and  $b_r$  in tuning the inertia channel and decoupler, which means adapting the inertia channel and decoupler dimensions in order to get the required resonance frequencies.

There are many disadvantages to the hydro mounts:

- Since it has to carry the static load of the car weight it is big and heavy
- In order to fulfill the requirements, the device is complicated (two chambers filled with a special liquid with a membrane and a channel separating them) and it is expensive.

Then, an air damped engine mount could be an issue to decrease the size of the damping device (it has only one chamber) and lower the price (it is quite simple and is based on air compression). But a pneumatic mount is less damped than the hydro mount and the damping has to be increased in order to damp heavy engines. In this report will be presented an overview about hydro-mechanical mount, pneumatic mounts and some tools that will be used to model the rubber dynamic properties, the air volume and the orifice behavior. After that, the model will be explained. Finally, some proposals how to increase the damping will be explained.

<b>I. INTRODUCTION.....</b>	<b>3</b>
<b>II. THE HYDROMOUNT FUNCTIONING AND MODELLING .....</b>	<b>5</b>
1. SCHEMA .....	5
2. PARAMETERS .....	5
3. HYDROMOUNT FUNCTIONING .....	6
4. FREQUENCY RESPONSE CHARACTERISTIC .....	6
5. MODELLING OF AN HYDROMOUNT WITH DECOUPLER .....	7
<b>III. PNEUMATIC SPRINGS: SOME EXAMPLES.....</b>	<b>11</b>
1. USED PARAMETERS AND CONSTANTS.....	11
2. DESCRIPTION OF A BASIC PNEUMATIC FLEXIBLE ELEMENT.....	12
3. SINGLE ACTION PNEUMATIC FLEXIBLE ELEMENT WITH DAMPING CHAMBER .....	12
<b>IV. MODELLING OF THE RUBBER .....</b>	<b>15</b>
1. USED PARAMETERS .....	15
2. RUBBER YOUNG’S MODULUS AND SHEAR MODULUS .....	15
3. DEFINITION OF THE ELASTIC STIFFNESS .....	16
4. DEFINITION OF DAMPING .....	17
5. PRESENTATION OF DIFFERENT VISCOELASTIC MODELS .....	18
<b>V. A MODEL OF THE ORIFICE IMPEDANCE .....</b>	<b>19</b>
1. PARAMETERS USED AND IMPEDANCE DEFINITION .....	19
2. INNER IMPEDANCE .....	20
3. RADIATION IMPEDANCE .....	22
<b>VI. ELECTRO- MECHANICAL-ACOUSTICAL ANALOGY.....</b>	<b>23</b>
<b>VII. THE MEASUREMENTS.....</b>	<b>25</b>
1. GENERAL SET-UP .....	25
2. STATIC MEASUREMENT .....	26
3. DYNAMIC MEASUREMENTS AND RESULTS.....	27
4. PNEUMATIC ENGINE MOUNT WITH CLOSED ORIFICE .....	28
5. THE PNEUMATIC ENGINE MOUNT WITH OPENED ORIFICE .....	29
<b>VIII. DESCRIPTION OF THE MODEL .....</b>	<b>30</b>
1. UNKNOWNNS AND ASSUMPTIONS .....	30
2. THE AIR COMPLIANCE EXPRESSION .....	31
3. THE RUBBER MODEL USED .....	31
4. THE BASIC EQUATIONS USED FOR THE FLUID.....	32
5. THE LIMITS OF THE MODEL.....	33
6. NUMERICAL IMPLEMENTATION IN MATLAB .....	33
7. PARAMETER STUDY .....	34
<b>IX. MODEL/MEASUREMENTS COMPARISON .....</b>	<b>36</b>
1. THE RUBBER MEASUREMENT AND MODEL COMPARISON .....	36
2. MEASUREMENTS AND MODEL FIT.....	36
<b>X. PROPOSALS HOW TO INCREASE THE DAMPING .....</b>	<b>38</b>
1. SEVERAL HOLES, ORIFICE AREA INCREASE.....	38
2. ACOUSTIC ABSORBENT INSIDE THE VOLUME.....	39
<b>XI. CONCLUSION AND DISCUSSION.....</b>	<b>40</b>
<b>REFERENCES .....</b>	<b>41</b>
<b>XII. APPENDIX A1: PARAMETER STUDY FOR –850 N PRELOAD AND 0.1 MM AMPLITUDE.....</b>	<b>42</b>
<b>XIII. APPENDIX A2: PARAMETER STUDY FOR –850 N PRELOAD AND 1 MM AMPLITUDE .....</b>	<b>46</b>
<b>XIV. APPENDIX B: CALCULATED AND MEASURED CURVES COMPARISON .....</b>	<b>50</b>
<b>XV. APPENDIX C: MATLAB CODE.....</b>	<b>56</b>



## II. The hydromount functioning and modelling

### 1. Schema

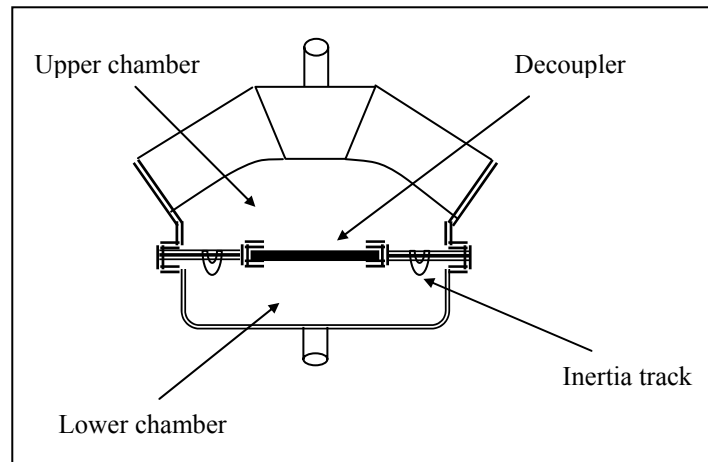


Figure 1: Schema of an hydromount

### 2. Parameters

With the help of the article [1], the useful parameters can be listed:

#### Parameters:

$A_d$	Diaphragm area, [m <sup>2</sup> ]
$A_i$	Cross-sectional area of the inertia track, [m <sup>2</sup> ]
$A_r$	Equivalent piston area of the rubber, [m <sup>2</sup> ]
$d_i$	Hydraulic diameter, [m]
$d_1, d_2$	Chambers diameters, [m]
$F$	Applied force, [N]
$\ell_i$	Effective length of the inertia track, [m]
$\ell_r$	Thickness of the rubber up, [m]
$m_E$	The engine mass, [kg]
$m_r$	Effective mass of the rubber in the shear mode, [g]
$p$	Pressure, [Pa]
$q_d, q_i$	Fluid flow rate through the decoupler and inertia track, [m <sup>3</sup> /s]
$x$	Displacement, [m]
$t_2$	Thickness of the rubber below, [m]
$V_1, V_2$	Chambers volumes, [m <sup>3</sup> ]

#### Constants

$B$	Bulk modulus of the fluid, [Pa]
$C_{d1}$	Equivalent linear compliance, [m <sup>5</sup> /N]
$E_r$	Young's modulus of rubber, [Pa]
$R_d$	Linear fluid resistance, [N/m <sup>5</sup> ]
$\mu$	Fluid viscosity, [Pa.s]
$\nu$	Poisson ratio, [-]
$\rho$	Fluid density, [kg/m <sup>3</sup> ]

Then other parameters can be computed using the geometry characteristics and the different constants.

Lumped fluid resistance	$R_i = \frac{128\mu\ell_i}{\pi d_i^4}$
Track inertance	$I_i = \frac{\rho\ell_i}{A_i}$
Fluid mass	$\rho V_1 \text{ and } \rho V_2$
Compliances	$C_{11} \approx A_r \ell_r \frac{1-3\nu^2-2\nu^3}{(1-\nu^2)E_r} + \frac{V_1}{2B_1}$
	$C_{12} \approx \frac{V_1}{2B_1} + C_d$
	$C_{21} = C_{22} \approx \frac{V_2}{2B_1} + \frac{\pi d_2^4}{16t_2 E_r}$
Inertances of the chambers	$\frac{m_1}{A_r^2}, \frac{m_2}{A_r^2}$

### 3. Hydromount functioning

In references [1] and [10], the functioning of a hydromount is described. The two chambers hydro-mechanical mount consists of two fluid chambers filled with glycol, which communicate through an orifice and an inertia track or a damping channel.

In the upper chamber, a steel casing and an elastomeric spring (primary rubber) supports the static load and are supposed to act uniaxially through the mount axis. The primary rubber also serves as a piston to pump the fluid through the rest of the mount.

The lower chamber, also made of rubber, is designed to be very soft and is used to absorb the transferred fluid without considerable pressure. Damping is created by the inertia effect of the fluid column resonating between the two springs.

The inertia track is a lengthy spiral channel that enables the fluid to pass from the upper chamber to the lower chamber. The inertia effect increases the dynamic stiffness. In fact, at high frequencies, the fluid doesn't follow the excitation and the orifice channel closes; the increasing pressure in the main chamber increases the stiffness.

The decoupler is a plastic plate. For small amplitude excitation, most of the fluid transport between chambers is via the decoupler orifice. For larger amplitude excitations, the decoupler is blocked and the most of the fluid flow is forced through the inertia track.

The geometry of the orifice channel (length, cross section), which determines the frequency of maximal angle and thus the damping properties, is used to tune the mount as a purpose of control. Some other important parameters determining the behavior of the entire mount are the hydraulic area and the volumetric stiffness.

### 4. Frequency response characteristic

The frequency response characteristic is described by J. E. Colgate et al. in [1]. Here is a summary:

- Below 5 Hz, the fluid flows between the chambers with low resistance.
- From 5 to 14 Hz and amplitude from 0.5 to 5.0 mm, these excitations are on the range of engine resonance and large enough to require significant damping. The resonance frequency of the system is on this range.

- From 25 to 250 Hz and amplitude from 0.05 to 0.5 mm, these excitations can cause noise and vibration and require good isolation. The resistance force to the fluid flow through the opening is greater than the elastic resistance of the rubber spring. The fluid pressure in the upper chamber fluctuates with excitation frequency but fluid pressure in the lower chamber remains almost constant.

### 5. Modelling of an hydromount with decoupler

In this part is explained how to draw a simple model of a hydro-mechanical mount with decoupler and how to get the parameters. It is also shown how to simplify a model for low frequency since a model for low frequencies has later to be derivate.

R. Singh et al. developed in [2] a lumped parameter model of a hydro-mechanical mount. Only vertical motions are taken into account here. The first step is to write the equation of motion and the momentum balance for each volume and mass involved in the model. The rubber is here modelled with Voigt model.

$$F^t \text{ is the total excitation force } F^t(t) = F_s + F(t) \quad (4.1)$$

$$x^t \text{ is the total displacement } x^t(t) = x_s + x(t) \quad (4.2)$$

The indice s stands for static conditions:  $F_s$  is the static load corresponding to the engine weight and  $x_s$  is the corresponding static displacement.  $F(t)$  and  $x(t)$  are the fluctuating components.

$k_r$  and  $b_r$  are assumed to be invariant with  $\omega$  and  $x^t$ .

The figure 2, which is a sketch of the forces acting on the mount, is related to the equations (4.3) to (4.10).

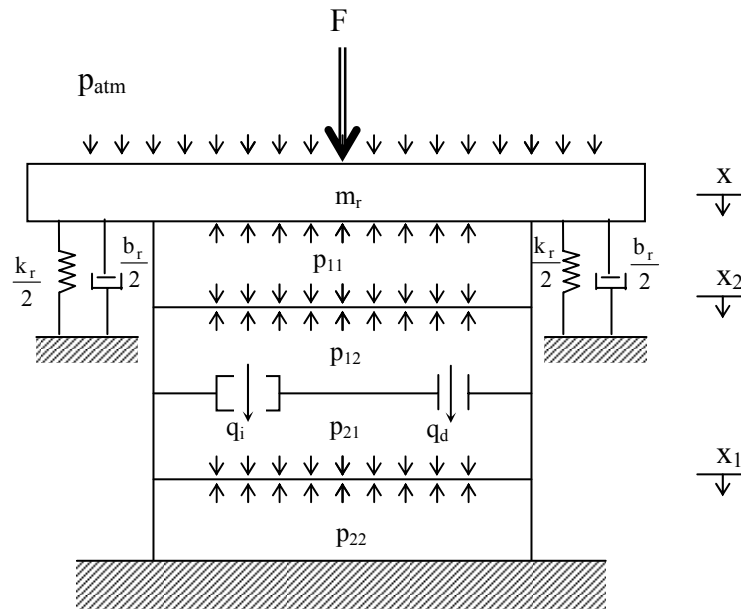


Figure 2: Schematic of a hydromount with a free decoupler

The equation of motion of the rubber mass can be written as:

$$F^t(t) - k_r x^t(t) - b_r \dot{x}^t(t) - A_r (p_{11}^t(t) - p_{atm}(t)) = m_r \ddot{x}^t(t) \quad (4.3)$$

The momentum balance applied to the fluid mass gives the three equations (4.4) to (4.6).

$$\text{For the fluid in the upper chamber } (p_{11}^t(t) - p_{12}^t(t))A_r = m_1 \ddot{x}_1^t(t) \quad (4.4)$$

$$\text{For the fluid in the lower chamber } (p_{12}^t(t) - p_{21}^t(t))A_r = m_2 \ddot{x}_2^t(t) \quad (4.5)$$

For the inertia track volume and the decoupler volume:

$$p_{12}^t(t) - p_{21}^t(t) = R_d q_d^t(t) = I_i \dot{q}_i^t + R_i q_i^t(t) \quad (4.6)$$

The equation of continuity applied to the compliant volume chambers gives, for the chamber 1:

$$A_r (\dot{x}_1^t(t) - \dot{x}_1^t(t)) = C_{11} \dot{p}_{11}^t(t) \quad (4.7)$$

$$A_r \dot{x}_1^t(t) - q_d^t(t) - q_i^t(t) = C_{12} \dot{p}_{12}^t(t) \quad (4.8)$$

Then for the chamber 2:

$$A_r \dot{x}_2^t(t) = C_{22} \dot{p}_{22}^t(t) \quad (4.9)$$

$$q_d^t(t) + q_i^t(t) - A_r \dot{x}_2^t(t) = C_{21} \dot{p}_{21}^t(t) \quad (4.10)$$

$C_{11}, C_{12}, C_{21}, C_{22}$ , are the compliances. The two first are the upper chamber compliances and the two last are the lower chamber compliances.

The static equilibrium gives:

$$F_s = k_r x_s + A_r (p_{11,s} - p_{atm}), \quad A_r x_s = (C_{11} + C_{12} + C_{21} + C_{22}) p_s \quad (4.11,12)$$

$$\text{and } A_r x_{1,s} = (C_{12} + C_{21} + C_{22}) p_s, \quad A_r x_{2,s} = C_{22} p_s \quad (4.13,14)$$

In considering the hydro-mechanical mount with a fixed decoupler (inactive decoupler), which means  $q_d(t)=0$  and eliminating the pressure variables, one gets the following time-varying equations

(4.15) to (4.18) with  $\dot{x}_i(t) = \frac{q_i(t)}{A_r}$ , and for the time varying part of the variables.

$$F(t) - \frac{A_r^2}{C_{11}} (x(t) - x_1(t)) - b_r \dot{x}(t) - k_r x(t) = m_r \ddot{x}(t) \quad (4.15)$$

$$\frac{A_r^2}{C_{11}} (x(t) - x_1(t)) - \frac{A_r^2}{C_{12}} (x_1(t) - x_i(t)) = m_1 \ddot{x}_1(t) \quad (4.16)$$

$$\frac{A_r^2}{C_{21}} (x_i(t) - x_2(t)) - \frac{A_r^2}{C_{22}} x_2(t) = m_2 \ddot{x}_2(t) \quad (4.17)$$

$$-R_i A_r^2 \dot{x}_i(t) + \frac{A_r^2}{C_{12}} (x_1(t) - x_i(t)) - \frac{A_r^2}{C_{21}} (x_i(t) - x_2(t)) = m_i \ddot{x}_i \quad (4.18)$$

Then, the analogous mechanical system can be drawn as seen in figure 3.

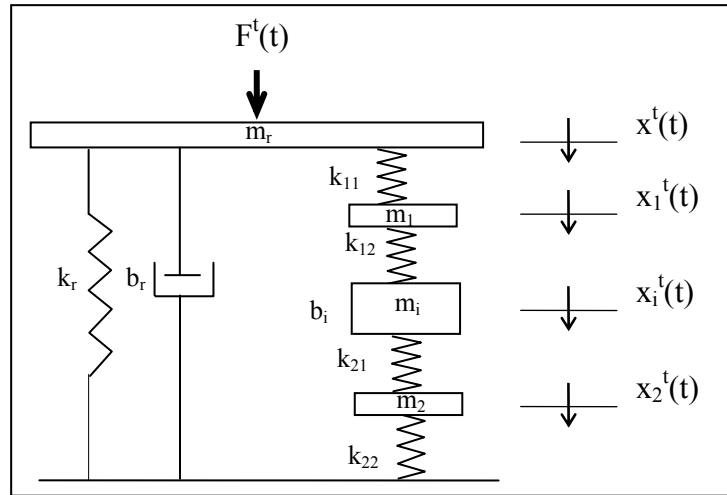


Figure 3: analogous mechanical system with free decoupler

The parameters are defined as:  $k_{11} = \frac{A_r^2}{C_{11}}$ ;  $k_{12} = \frac{A_r^2}{C_{12}}$ ;  $k_{21} = \frac{A_r^2}{C_{21}}$ ;  $k_{22} = \frac{A_r^2}{C_{22}}$  and  $m_i = A_r^2 I_i$ ;  $b_i = A_r^2 R_i$ .

The different k correspond to the chamber stiffness, the mass  $m_r$  to the rubber mass,  $m_1$  and  $m_2$  to fluid mass in the chamber 1 and 2 respectively.  $b_i$  corresponds to the inertia track resistance.

Then, in [2] again, the equations are simplified for low frequency. In fact, the impedances of the lumped fluid masses are negligible at low frequencies and a two-degree-of-freedom model can be derived. Then, there will only be two compliances  $C_1$  and  $C_2$ , which can be calculated as the sum  $C_{11}+C_{12}$  and  $C_{21}+C_{22}$  respectively. Moreover,  $p_{11}(t) \approx p_{12}(t) = p_1(t)$  and  $p_{21}(t) \approx p_{22}(t) = p_2(t)$ .

$$F(t) - k_r x(t) - b_r \dot{x}(t) - A_r p_1(t) = m_r \ddot{x}(t) \quad (4.19)$$

$$p_1(t) - p_2(t) = R_d q_d(t) = I_i \dot{q}_i(t) + R_i q_i(t) \quad (4.20)$$

$$A_r \dot{x}_1(t) - q_d(t) - q_i(t) = C_1 \dot{p}_1(t) \quad (4.21)$$

$$q_d(t) + q_i(t) = C_2 \dot{p}_2(t) \quad (4.22)$$

In eliminating the variables  $p_1(t)$  and  $p_2(t)$  and with  $\dot{x}_i(t) = \frac{q_i(t)}{A_r}$  one gets:

$$F(t) - \frac{A_r^2}{C_1} (x(t) - x_i(t)) - b_r \dot{x}(t) - k_r x(t) = m_r \ddot{x}(t) \quad (4.23)$$

$$-R_i A_r^2 \dot{x}_i(t) + \frac{A_r^2}{C_1} (x(t) - x_i(t)) - \frac{A_r^2}{C_2} x_i(t) = m_i \ddot{x}_i(t) \quad (4.24)$$

Then, a simplified model for hydromount with fixed decoupler (which correspond to low frequency), can be drawn as in figure 4.

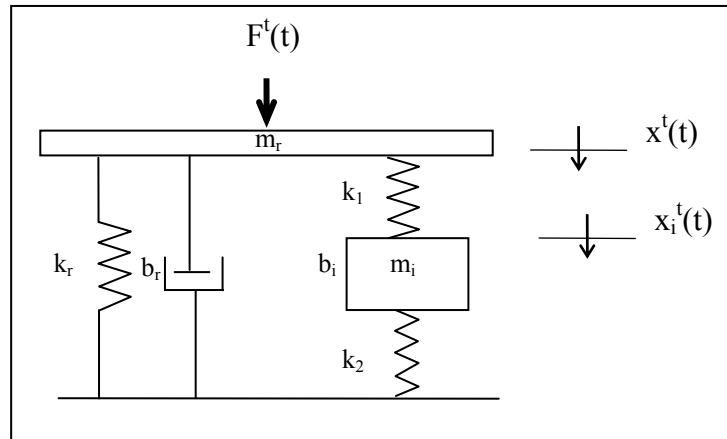


Figure 4: analogous mechanical system with fixed decoupler

This was however a linear model and it is possible to use it because high and low frequencies can be separated and then get two linear models in order to cover the entire frequency range. But it is sometime required to derivate a non-linear model. A. Geisenberg et al., in [12], explain how to get a non-linear model in enhancing the parameters of the linear model discussed above. The parameters identification via experiment is also well described in this paper.

### III. Pneumatic springs: some examples

In this chapter will be described two simple pneumatic springs: a basic cylinder piston element and a single action pneumatic element with damping chamber. In both cases the stiffness will be derived.

#### 1. Used parameters and constants

##### Parameters

A	Piston cross-sectional area, [m <sup>2</sup> ]
d	Diameter of the capillary, [m]
F	External applied force, [N]
h	Height (smaller dimension), [m]
ℓ	Length of the capillary, [m]
m	Mass of preload, [kg]
T <sub>0</sub>	Initial temperature, [K]
w	Width (larger dimension), [m]
Q	Volume flow rate, [m <sup>3</sup> /s]
V	Instantaneous internal volume between piston and cylinder, [m <sup>3</sup> ]
W	Weight flow rate (W=Q.g), [N/s]
v	Flow velocity, [m/s]

##### Constants

g	Gravity acceleration, [m/s <sup>2</sup> ]
p <sub>atm</sub>	Atmospheric pressure, P <sub>atm</sub> =101300 Pa for the air
R	Universal gas constant, R=286.4 N-m/(kg K) for the air
γ	Ratio of specific heats, γ=1.3 for the air
μ	Dynamic viscosity of the gas, [Pa.s]
ρ	Gas density, [kg/m <sup>3</sup> ]

Computed parameters:

Reynolds number	
Round capillary:	$Re = \frac{vd\rho}{\mu}$
Rectangular capillary:	$Re = \frac{Q}{wh} \frac{\rho}{\mu} = \frac{Q\rho}{w\mu}$
Capillary resistance	
Round capillary:	$C_c = \frac{\pi d^2}{128\mu\ell}$
Rectangular capillary:	$C_c = \frac{wh^2}{12\mu\ell}$
Initial pressure	$p_i = p_{atm} + \frac{mg}{A}$

## 2. Description of a basic pneumatic flexible element

The book [7] describes among other systems of vibration isolation, pneumatic flexible element, which are using compressed air as flexible element. The more simple is a linear cylinder-piston system. The piston is moving into the cylinder, which can be of any cross-sectional shape. The figure 5 shows a schema of the device.

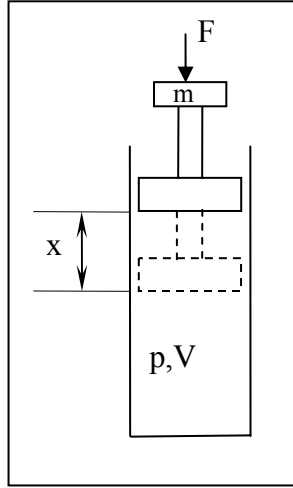


Figure 5: basic pneumatic flexible element

Assuming an adiabatic compression yield:  $p_i V_i^\gamma = p_x V_x^\gamma$  (5.2)

$p_x$  and  $V_x$  are the absolute pressure and volume after the piston moved by  $x$ .

The pressure and the volume can be expressed as below:

$$p = \frac{F}{A}, V_x = V_i - Ax \quad (5.2,3)$$

In assuming that the piston surface area is constant, the stiffness of the pneumatic flexible element is finally:

$$k_0 = \frac{dF}{dx} = \frac{\gamma p_i A^2}{V_i} \left[ \frac{1}{1 - \left(\frac{A}{V_i}\right)x} \right]^{\gamma+1} \quad (5.4)$$

$$\text{If } Ax \ll V_i: k_0 \cong \frac{\gamma p_i A^2}{V_i} \quad (5.5)$$

And for pneumatic isolators, usually  $p_0 = \frac{F_0}{A} = \frac{mg}{A} \gg p_{\text{atm}}$

The stiffness is then approximately proportional to the weight of the supported object; the pneumatic flexible element has a natural “constant natural frequency” characteristic.

The equation (5.4) will be used as a model of the air volume stiffness of the pneumatic mount.

## 3. Single action pneumatic flexible element with damping chamber

Another more complicated passive pneumatic vibration isolator is a self-damped pneumatic spring (which itself has no significant damping) in which the main cylinder is connected with a damping chamber through a capillary. This device is described in [7] by I. Rivin. It is shown in figure 6.



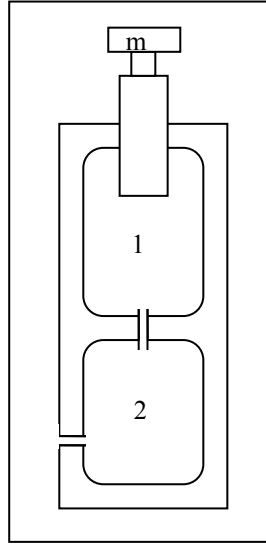


Figure 6: Single action pneumatic flexible element with damping chamber

The flow through a capillary, for a passage whose length is much greater than its cross sectional dimension, e.g. the diameter, is:  $W_{t1} = \frac{gC_c}{2RT_0}(p_1^2 - p_2^2)$  (5.6)

which can be linearized as:  $W_{t1} = \frac{p_i g C_c}{RT_0}(p_1 - p_2)$  (5.7)

since for small oscillations and laminar flow:  $p_1 + p_2 \approx 2p_i$

The Reynolds number is able to give an idea about the fluid behavior. The flow can be assumed linear if the Reynolds number  $Re < 2000$  (which corresponds to a low fluid flow velocity and/or a high viscosity) or, in taking a prudent safety margin,  $Re < 500$ .

Since the weight flow rate from the damping chamber 2 can be expressed as:

$$W_{t1} = -\frac{gV_3}{\gamma RT_0} \frac{dp_3}{dt} \quad (5.8)$$

$W_{t1}$  can be recalculated in putting the expression of  $p_3$  from the equation (5.7) into (5.8), which gives:

$$W_{t1} = -\frac{gV_3}{\gamma RT_0} \left( \frac{RT_0}{gp_i C_c} \frac{dW_{t1}}{dt} + \frac{dp_1}{dt} \right) \quad (5.9)$$

The weight flow rate into the chamber 1 is:  $W_{t1} = -\frac{g}{RT_0} \left( \frac{V_{t1}}{\gamma} \frac{dp_1}{dt} + p_1 \frac{dV_{t1}}{dt} \right)$  (5.10)

Since one can approximate:  $p_1 = p_i + \Delta P$ ,  $V_1 = V_i - Ax$  and that one can assume:  $Ax \ll V_i$  and  $\Delta p_1 \ll p_i$ :

$$W_{t1} = \frac{g}{RT_0} \left( \frac{V_i}{\gamma} \frac{dp_1}{dt} - p_i A \frac{dx}{dt} \right) \quad (5.11)$$

The dynamic stiffness is finally found after calculations and for sinusoidal excitation:

$$k = \frac{Dp}{Dx} = k_0 \frac{1 + N \frac{j\omega}{\omega_0}}{1 + N + N \frac{j\omega}{\omega_0}} \quad (5.12)$$

$$\text{with } N = \frac{V_3}{V_i} \text{ and } \omega_0 = \frac{\gamma C_c p_i}{V_i} = \frac{C_c}{A^2} k_0$$

## IV. Modelling of the rubber

It is important to know how to model the main part of the pneumatic mount, which is the rubber piston. Papers about the behavior of such elastic material are summarized and the equations used to model it are given.

### 1. Used parameters

Below is a list of the used parameters:

a	Indenter radius, [m]
$c_s$	Young's modulus, [Pa]
d	Indent penetration depth, [m]
E	Young's modulus, [Pa]
$E^*$	Viscoelastic parameter, [Pa]
F	Applied force, [N]
G	Shear modulus
k	Stiffness, [N/m]
t	Time, [s]
x	Displacement, [m]
$\varepsilon$	Strain, [-]
$\sigma$	Stress, [Pa]
$\omega$	Angular frequency, [rad/s]
$\theta$	Conical indenter, semi-angle, [°]

### 2. Rubber Young's modulus and shear modulus

In [16] are described two parameters used to quantify some of the rubber properties:

- The shear modulus G describes the resistance to a simple shearing stress
- The Young's modulus of elasticity E is the ratio of a simple tensile stress to the corresponding fractional tensile elongation.

The relation between those two values is:  $E = 2G(1 + \nu)$ .  $\nu$  is the Poisson's ratio, which is defined by the ratio of lateral contraction to longitudinal tension.

Under small deformation rubbers are linearly elastic solids. Because of high moduli of bulk compression compared with the shear moduli, they may be regarded as relatively incompressible. The elastic behaviour under small strains can thus be described by a single elastic constant G since  $E = 3G$  in this case.

It is common to characterize the modulus, stiffness or hardness of rubber by measuring their elastic indentation by rigid indenter of prescribed size and shape, pressed into the surface, under specific loading conditions. The indentation hardness is inversely related to the penetration and is dependent on the modulus of elasticity and the viscoelastic properties of the material. There are various different non-linear scales used to derive rubber hardness from such measurements. One is the Shore hardness A: the units of hardness range from 0 for the full protrusion of the indenter to 100 for nil protrusion. Another one is the IRHD (International Rubber Hardness Degrees).

The formula relating the force F and the shear modulus G for the different indentors are given in the book [16]:

For a spherical indenter of radius a:  $F = \frac{16}{3}Ga^{1/2}d^{3/2}$

For a flat-ended cylindrical indenter of radius a:  $F = 8Gad$

For a conical indenter with semi-angle  $\theta$ :  $F = \frac{8}{\pi} Gd^2 \tan(\theta)$

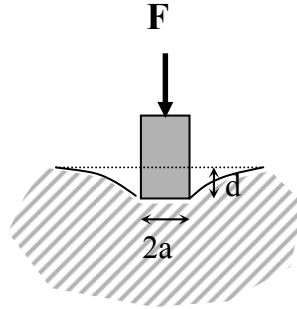


Figure 7: Indentation by a flat ended indenter

Some values of Young modulus  $E$  related to specific hardness, and for different hardness scales are shown in table 1.

Hardness (degrees)	E (Shore) [MPa]	E (IRHD) [Mpa]
10	0.4	0.3
20	0.7	0.6
30	1.2	1.0
40	1.7	1.5
50	2.5	2.3
60	3.8	3.6
70	6	5.5
80	10	9.5
90	23	20

Table 1: Relation between indentation hardness and elastic Young modulus

### 3. Definition of the elastic stiffness

In [3] Shi-Jian Zhu et al. give in a first part a definition of the elastic stiffness that can be used in engineering and especially for rubber.

The stiffness of elastic body is defined as partial differential of the acting force on the elastic body to its corresponding displacement:

$$k = \frac{\partial F}{\partial x} \tag{6.1}$$

If the displacement depends only on the acting force and its time history, the stiffness is then a function of the displacement and its derivative:

$$k = \frac{\partial F}{\partial x} = k(x, \dot{x}, \ddot{x}, \dots) \tag{6.2}$$

In engineering, different forms of stiffness are needed: the static stiffness, the dynamic stiffness and the shock stiffness. They correspond respectively to static load, dynamic load and shock load. For rubber, the values of those three kinds of stiffness are really different. The standard three-parameters solid model describes qualitatively the stiffness with respect to very limited range of frequency characteristics in a broader range of mechanism.

In order to describe the stiffness frequency characteristic in a broader range of frequency, more retardation mechanism that work at different frequencies should be considered in this model.

In vibration engineering, the stiffness can be defined by the displacement response to a sine force excitation, for instance  $F(t) = Fe^{j\omega t}$  (with an amplitude  $F$  and a frequency  $\omega$ ), on an elastic body.

The steady displacement response can be written as  $X(t) = Xe^{j\omega t + \phi} = X^* e^{j\omega t}$ . The complex stiffness can then be derived as  $k^* = \frac{F}{X^*} = k^*(\omega, X)$ . The static stiffness, dynamic stiffness and shock

stiffness can all be obtained from the complex stiffness. The above definition is based on the assumption that the initial displacement, velocity and acceleration are all zero before loading.

If the relation between the force and the deformation is approximately linear, the application of a sinusoidal deformation will result in a sinusoidal force of the same frequency but displaced in terms of phase by an amount termed the loss angle. It is convenient to consider the elastic (in phase response) and the viscous (out-of-phase response) in terms of two modules. The overall response can be expressed as a complex number  $G^* = G' + jG''$ . The dynamic stiffness is given by  $k = |G^*|$ , and the phase or loss angle  $\delta$  by  $\tan\delta = G''/G'$ .

The stiffness of natural rubber is increasing lightly with frequency. This is called “dynamic stiffening”.

#### 4. Definition of damping

According to [4], damping is the phenomenon by which mechanical energy is dissipated in dynamic systems. Then, in [4] is also discussed different type of damping and how to model them. Since in our pneumatic damper, there is material damping in the rubber, an overview of the information found about material damping is given in the following.

Internal damping of materials originates from the energy dissipation associated with microstructure defects, such as:

- Grain boundaries and impurities
- Thermoelastic effects caused by local temperature gradients resulting from non-uniform stresses
- Eddy-current effects in ferromagnetic materials, dislocation motion in metals
- Chain motion in polymers.

The equations for the different models described in the next paragraph are:

$$\text{For the Kelvin-Voigt model (see table 2): } \sigma = E\varepsilon + E^* \frac{\partial\varepsilon}{\partial t} \quad (6.5)$$

$$\text{For the Maxwell model (see table 2): } \sigma + c_s \frac{d\sigma}{dt} = E^* \frac{\partial\varepsilon}{\partial t} \quad (6.6)$$

$$\text{For the standard linear solid model (see table 2): } \sigma + c_s \frac{d\sigma}{dt} = E\varepsilon + E^* \frac{\partial\varepsilon}{\partial t} \quad (6.7)$$

More specifically for rubber:

Energy dissipation through hysteresis is represented by the area between the loading and unloading curves in load deformation cycle, and occurs with all rubbers. It depends on the type of polymer, of the filler and the other compounding ingredients. The degree of damping is commonly expressed in terms of the loss angle.

### 5. Presentation of different viscoelastic models

Different model of viscoelasticity are compared in [3]: Maxwell model, Voigt model and the standard solid model. The described models are based on elastic springs obeying Hook's law and viscous dashpot obeying Newton viscosity law.

Schematic representations of those models are given in table 2.

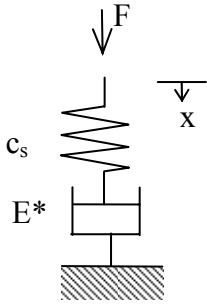
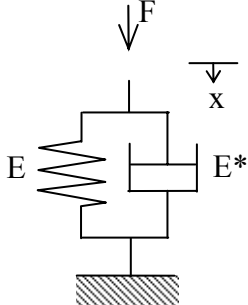
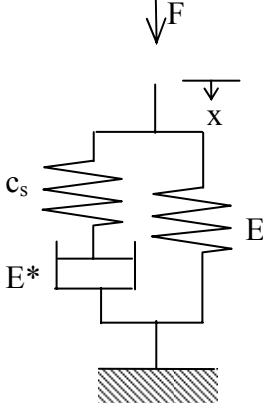
Maxwell model	Voigt model	Standard solid model
		
$\sigma + c_s \frac{d\sigma}{dt} = E^* \frac{\partial \varepsilon}{\partial t}$	$\sigma = E\varepsilon + E^* \frac{\partial \varepsilon}{\partial t}$	$\sigma + c_s \frac{d\sigma}{dt} = E\varepsilon + E^* \frac{\partial \varepsilon}{\partial t}$

Table 2: different mechanical models of rubber

In ref [3], it is discussed that for actual viscoelastic body, the range of frequency affecting the stiffness is wide. Hence, it is impossible to be only one retardation mechanism in the range. There should be a series of retardation mechanisms with different characteristic frequencies and the associated weight factors must be different. The standard three-parameters solid model can be generalized to the general Maxwell model consisting of a series of Maxwell bodies connected in parallel. Every Maxwell body represents a retardation mechanism with certain characteristic frequency. The spring connected with too ends directly as a stiffness appearing as a static stiffness. The number of elements is determined based on the frequency section interested. It is clearly shown than the more elements are used, the more accurate fitting is reached. Then, the Voigt model can be used because it is quite easy to do so, but in order to improve the global model, a general Maxwell model with many elements would be better.

## V. A model of the orifice impedance

### 1. Parameters used and impedance definition

A	Orifice cross section area, [m <sup>2</sup> ]
$\ell$	Length of the orifice, [m]
p	Pressure, [Pa]
r	Radius of the orifice, [m/s]
R	Real part of the impedance, [Ns/m <sup>5</sup> ]
U	Volume flow, [m <sup>3</sup> /s]
v	Particle velocity in the orifice (the velocity due to the difference of pressure on two sides of orifice), [m/s]
X	Imaginary part of the impedance, [Ns/m <sup>5</sup> ]
Z	Impedance, [Ns/m <sup>5</sup> ]
$\lambda$	Viscosity wavelength, [m]
$\omega$	Angular frequency, [rad/s]
$\Psi$	Negative pressure gradient parallel to the axis of the tube
$\xi, \dot{\xi}, \ddot{\xi}$	Displacement, velocity, [m,m/s] acceleration, in the x direction [m/s <sup>2</sup> ]
c	Sound speed, c=343 m/s in the air
$\mu$	Coefficient of viscosity, $\mu=17.98 \cdot 10^{-6}$ Pa.s for the air
$\rho$	Density, $\rho=1.2255$ kg/m <sup>3</sup> for the air

The different wave numbers:

$$k = \sqrt{-\frac{j\omega\rho}{\mu}}$$

$$k_2 = \beta = \sqrt{\frac{\omega\rho}{2\mu}}$$

$$k_3 = \frac{\omega}{c}$$

The acoustical impedance at a given surface is defined as the complex ratio of effectiveness sound pressure average over the surface to effective volume velocity through it:  $Z_A = \frac{p}{U}$ . The unit is Newton-second/m<sup>5</sup>, or mks acoustic ohms. Since the impedance is complex, an other expression is:  $Z_A=R_A+jX_A$ .

## 2. Inner impedance

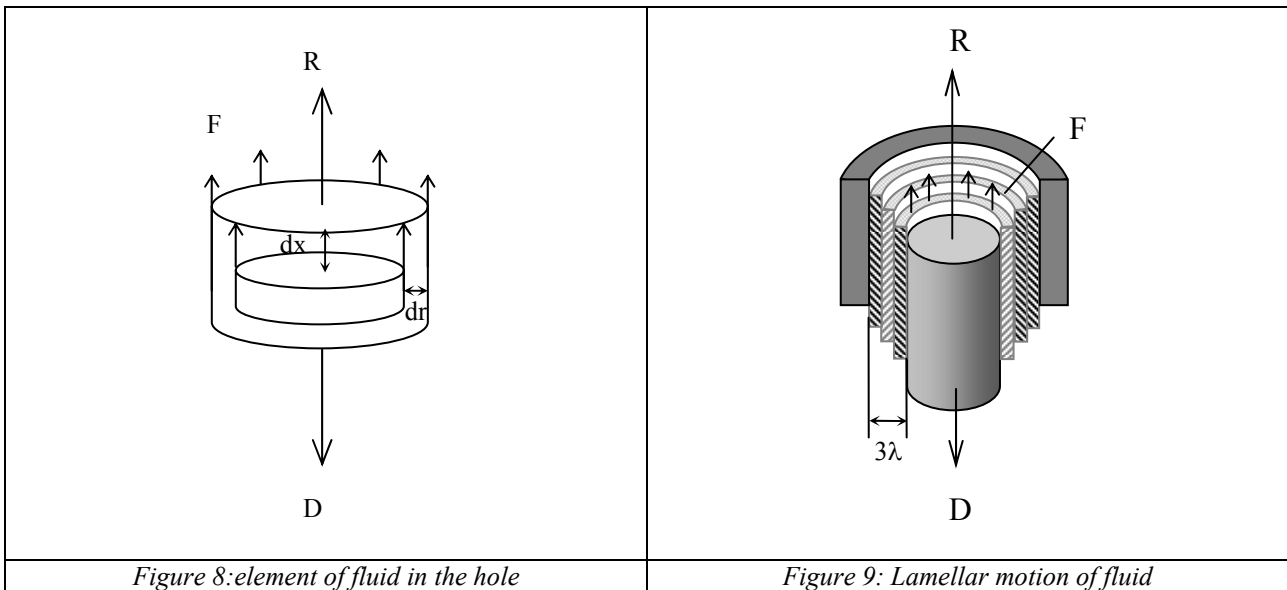


Figure 8: element of fluid in the hole

Figure 9: Lamellar motion of fluid

In a moderately large tube, B. Crandall explains in [15] that the viscosity waves are diffused radially from the fluid, where the velocity is the greatest, to the walls of the tube, where the velocity is nil. One property of those waves is that there are almost extinguished after traversing a distance

of one wavelength,  $\lambda = \frac{2\pi}{\beta} = 2\pi \sqrt{\frac{2\mu}{\rho\omega}}$ . Then, the effect of viscosity for sound waves wider than

double this wavelength is confined to a layer near to the wall of thickness approximately one wavelength (see figure 9). In the center of the tube, the dragging effect is absent, which means that the axial velocity doesn't vary much with the distance from the center: it can be seen as a cylinder core of air, oscillating in the center of the tube, as seen in figure 9. The reaction from the layer between the air cylinder and the wall affects the motion of this air cylinder. Then, added inertia and resistance are involved. To derive the impedance, the equation of motion has to be written and first the forces acting in a piece of air (see figure 8) are:

- The axial driving forces acting on a circular membrane (D) is  $\Psi dx$  per unit area.  $\psi$  is the negative pressure gradient parallel to the axis of the tube. For a volume  $2\pi r dr dx$  it is written  $\Psi dx \cdot 2\pi r dr$ .
- The opposed reactance due to inertia (R):  $j\omega\rho 2\pi r dr dx$ .
- The opposing friction force on the inner surface of the ring (F) is:  $-2\pi r dx \cdot \mu \frac{\partial \dot{\xi}}{\partial r}$ . The net

force on the annulus due to friction is then:  $\frac{\partial}{\partial r} \left( -2\pi r dx \cdot \mu \frac{\partial \dot{\xi}}{\partial r} \right) dr$ .

The equation of motion can be written:

$$\left[ j\omega\rho - \frac{\mu}{r} \frac{\partial}{\partial r} \left( r \frac{\partial}{\partial r} \right) \right] \dot{\xi} = \psi \quad (7.1)$$



Since only  $\xi$  is dependent on  $r$ , the equation (7.1) may be rewritten as:

$$\left[ \frac{\partial^2}{\partial r^2} + \frac{1}{r} \frac{\partial}{\partial r} + k^2 \right] \xi = -\frac{\Psi}{\mu} \quad (7.2)$$

The solution of this differential equation, in taking into account that the velocity must vanish at the boundary  $r=r_0$ , is:

$$\xi(r) = -\frac{\Psi}{\mu k^2} \left[ 1 - \frac{J_0(kr)}{J_0(kr_0)} \right] \quad (7.3)$$

Integrating the last equation over the section gives the mean velocity:

$$\bar{\xi}(r) = -\frac{\Psi}{\mu k^2} \left[ 1 - \frac{2J_1(kr_0)}{kr_0 J_0(kr_0)} \right] \quad (7.4)$$

Then the impedance can be calculated.  $\Psi \ell$  is the total pressure acting on the circular membrane and  $\bar{\xi} \pi r^2$  is the velocity in the section. The impedance, defined as  $Z_i = \frac{\Psi \ell}{\bar{\xi} \pi r^2}$  is then:

$$Z_i = \frac{\ell}{\pi r^2} j \omega \rho \frac{1}{1 - \frac{2 J_1(kr)}{kr J_0(kr)}} \quad (7.5)$$

In order to evaluate the impedance for values of  $|kr|$  in the range  $1 < |kr| < 10$ , the relation  $\frac{J_1(\alpha \sqrt{-j})}{J_0(\alpha \sqrt{-j})} = -j$ , with  $\alpha \sqrt{-j} = r \sqrt{\frac{-j \omega \rho}{\mu}}$  and for  $\alpha > 10$ , can be applied. The impedance can be then reduced to the more simple expression:

$$Z_i = \left( j \omega \rho + \frac{2 \mu \beta}{r} (1 + j) \right) \frac{\ell}{\pi r^2} \quad (7.6)$$

Since in our case, for 30 Hz,  $|kr| = \alpha = 3.6$ , the equation (7.6) can be used to build the model parameters.

From [12], the inner impedance of a small orifice whose length and diameter are comparable in size can be written as:

$$Z_i = \frac{\ell}{\pi r^2} j \omega \rho \frac{1}{1 - \frac{2 J_1(k_2 r (-2j)^{1/2})}{k_2 r (-2j)^{1/2} J_0(k_2 r (-2j)^{1/2})}} + 0.5 \frac{\rho |v|}{A} \quad (7.7)$$

This is actually the same expression than the previous one but including a non linear term  $0.5 \frac{\rho |v|}{A}$  taking into account that the impedance is increasing with the air particle velocity,  $v$ , in the hole. In fact, in [12], the real part of the impedance is plotted for different speed flow in the orifice and it is pointed out that the nonlinearity that can be seen is a velocity effect rather than amplitude or acceleration effect.

### 3. Radiation impedance

The radiation mechanical impedance of a plane piston on infinite baffle,  $Z_{Mr}$ , is defined by Beranek in Ref [5]. The acoustical impedance  $Z_{Ar}$  is then:

$$Z_{Ar} = Z_{Mr}/(\pi r^2)^2 ; Z_{Ar} = \frac{\rho c}{\pi r^2} \left( 1 - \frac{J_1(2k_3 r)}{k_3 r} + j \frac{H_1(2k_3 r)}{k_3 r} \right) \quad (7.8)$$

In the formula above,  $k_3 = \omega/c$  is the wave number.  $J_1$  is the Bessel function of first order and  $H_1$  is the Struve function of order one. Since there is no readily available Struve function in MATLAB, one has to approximate the Struve function with the firsts terms of the power series expansion:

$$H_1(z) = \frac{2}{\pi} \left( \frac{z^2}{1^2 3} - \frac{z^4}{1^2 3^2 5} + \frac{z^6}{1^2 3^2 5^2 7} - \dots \right)$$

Another approximation could also be, from [14]:

$$H_1(z) \approx \frac{2}{\pi} - J_0(z) + \left( \frac{16}{\pi} - 5 \right) \frac{\sin(z)}{z} + \left( 12 - \frac{36}{\pi} \right) \frac{1 - \cos(z)}{z^2}$$

But the difference occurs at high frequency and the frequency range we are working on is from 0 to 30 Hz; then the final result is not changed and either of these expressions could be used.

In the figure 10 below is drawn the real and imaginary part of the mechanical impedance of a piston in infinite baffle in logarithmic scale as in Ref [5].

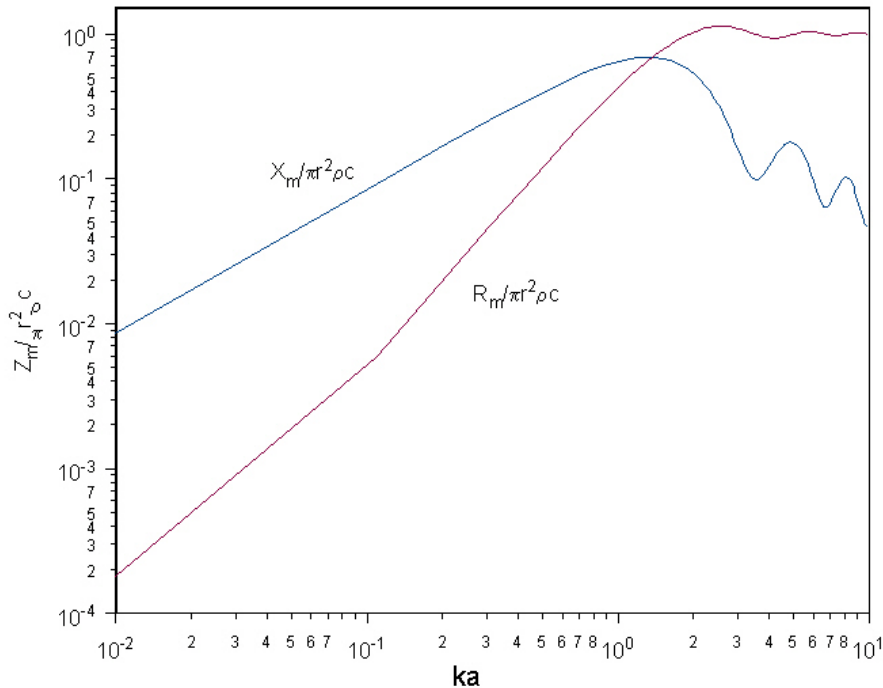


Figure 10: Real and imaginary part of the normalized mechanical impedance of the air load on one side of a plane piston mounted in an infinite flat baffle

## VI. Electro- mechanical-acoustical analogy

It could be useful to make an electro-mechanical-acoustical analogy, which means applying the electrical-circuit theory to the solution of mechanical and acoustical problems. In [5] an electrical analogy for mechanical and acoustic mass, compliance and resistance are largely discussed. In fact, they are the basic element that should be combined in order to get more complicated devices.

That is why, with the help of [5] the impedance-type analogy for acoustical mass, acoustical compliance and acoustical resistance will be shown here in the table 4 below.

To transform a physical law into acoustical terms, one uses the formula:  $p(t) = \frac{f(t)}{S}$  where p is the pressure, f the force and S the section area.

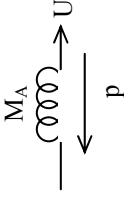
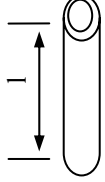
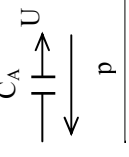
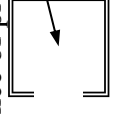
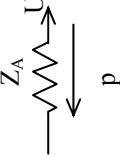
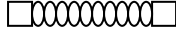
Acoustical element	Unit	Impedance-type analogy and symbol	Equations		Acoustical element
			Physical law converted into acoustical terms:	Steady state ( $\omega = 2\pi f$ )	
Mass	Kg/m	Inductance (L) 	$p(t) = M_A \frac{dU(t)}{dt}$	$p = j\omega M_A U$	Tube filled with gas of length $l$ and cross-sectional area $S$ . 
Acoustical compliance	m/N	Capacitance (C <sub>E</sub> ) 	$p(t) = \frac{1}{C_A} \int U(t) dt$	$p = \frac{U}{j\omega C_A}$	Enclosed volume of air $V$ with opening for entrance of pressure variations. 
Acoustical resistance	N/sm	Resistance (R <sub>E</sub> ) 	$p(t) = R_A U(t)$	$p = R_A U$	Fine-mesh screen 
Any impedance				$Z = \frac{p}{U}$	

Table 4: Acoustical-Electrical analogies

## VII. The measurements

Here is explained how the measurements have been done and the interpretation of them in order to build the model.

### 1. General set-up

The dynamics measurements are done on a servo-hydraulic machinery (MTS-1000 Hz). This machinery is behaving rigid up to high frequencies (1000 Hz at least) in order to avoid bending waves in the set-up. The machinery can do measurements up to 1000 Hz.



*Figure 11: Measurement set-up: the servo-hydraulic machinery*

The displacement is given and measured at the upper side of the piston of the mount. The resulting force at the steel plate is measured. With those data, the stiffness can be calculated in two ways:

- Calculate the peak-to-peak value of the force and displacement signal, which gives the absolute value of the dynamic stiffness. The phase is calculated out of the actual hysteresis curve area.
- The second method is to use the fast Fourier transform. The amplitude of the fundamental wave is calculated. The phase shift is the difference of the load phase and the displacement phase.

To validate the model, different measurements are done. Three preloads are chosen: -850 N, -1000 N and -1200 N (it covers different type of vehicle in which the damper could be mount in) and two excitation amplitude: 1 mm and 0.1 mm (it covers different driving conditions and different roads types). The chosen frequency range is from 0 to 30 Hz.

The dynamic stiffness measurements are first done on the mount described on chapter IV. Then, the dynamic stiffness measurements are also done for a closed orifice and for an orifice of 20 mm of diameter in order to test the total mount highest and lower stiffness limits. In all the following plots, the frequency is in Hertz, the absolute value of the stiffness in N/m, and the angle in degrees.

## 2. Static measurement

The static measurements are done in a spindle machinery. The speed given is then very well controlled. Since this machinery is not completely stiff, a sensor is measuring the force due to this lack of stiffness and the results are then more accurate by updating with the sensor data.

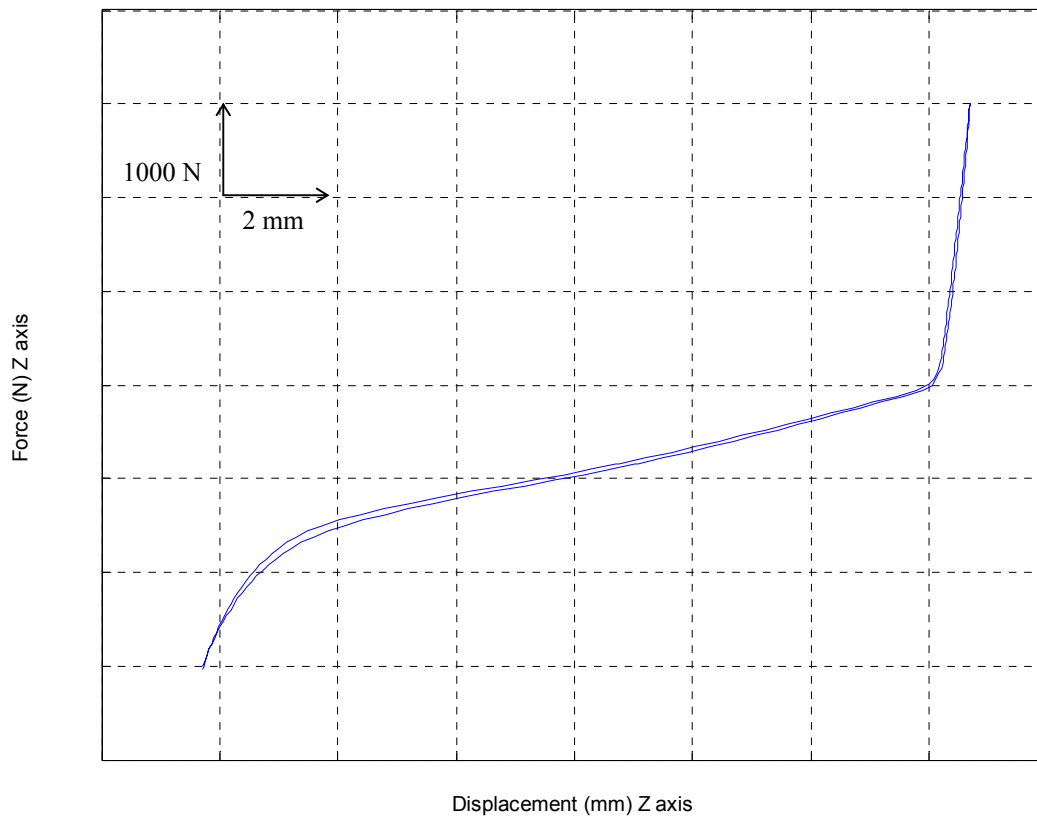


Figure 12: Force-displacement curve

### 3. Dynamic measurements and results

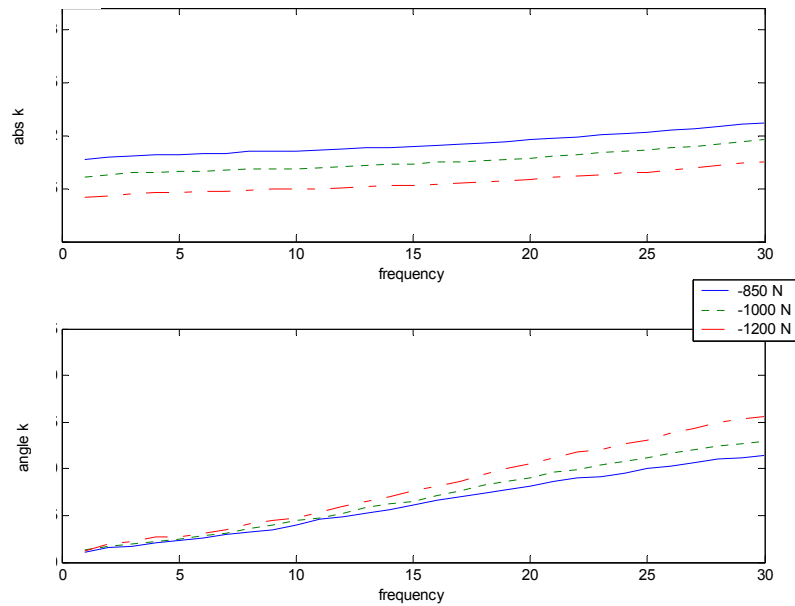


Figure 13: Measured dynamic stiffness and phase angle for 0.1 mm amplitude excitation

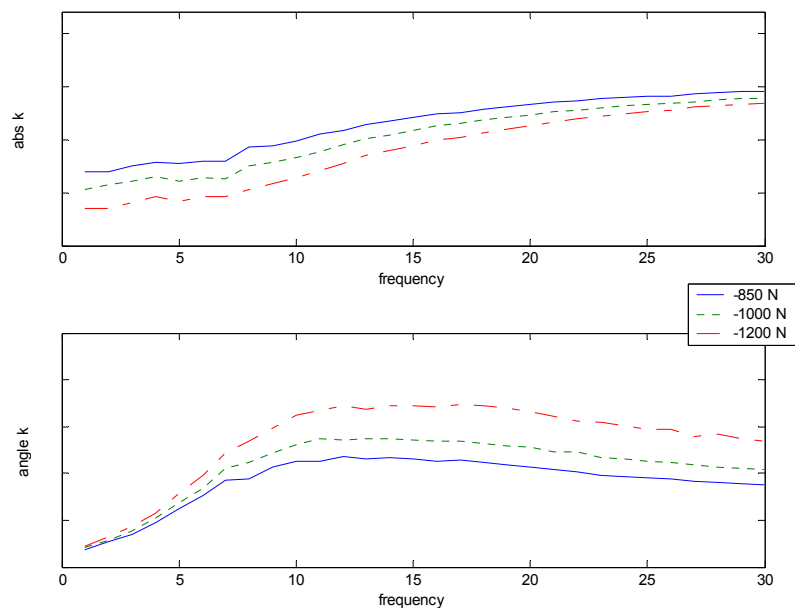


Figure 14: Measured dynamic stiffness and phase angle for 1 mm amplitude excitation

Out of those measurements (figure 13 and 14), one can see that the amplitude of excitation plays a big role.

In plotting the curves of the absolute value and the phase angle of the complex stiffness for different preload on the same graph, one can also see a preload influence. The preload has an influence on the working chamber volume. In fact, if the preload increases, the chamber volume decreases, which result in a lower compressibility of the air enclosed volume and to higher stiffness. But the shift of the absolute value to lower values when the preload increases is also due to the rubber dependence on preload, which is not modelled.

#### 4. Pneumatic engine mount with closed orifice

Before closing the orifice, a deflection is imposed to the mount. A deflection of 5.5 mm corresponds to  $-850$  N preload, a deflection of 6.5 mm corresponds to  $-1000$  N preload, and finally, a deflection of 7.5 mm corresponds to  $-1200$  N preload. Then, after closing the orifice, the pressure inside the mount is the atmospheric pressure. Thereafter, the dynamic measurements can be done.

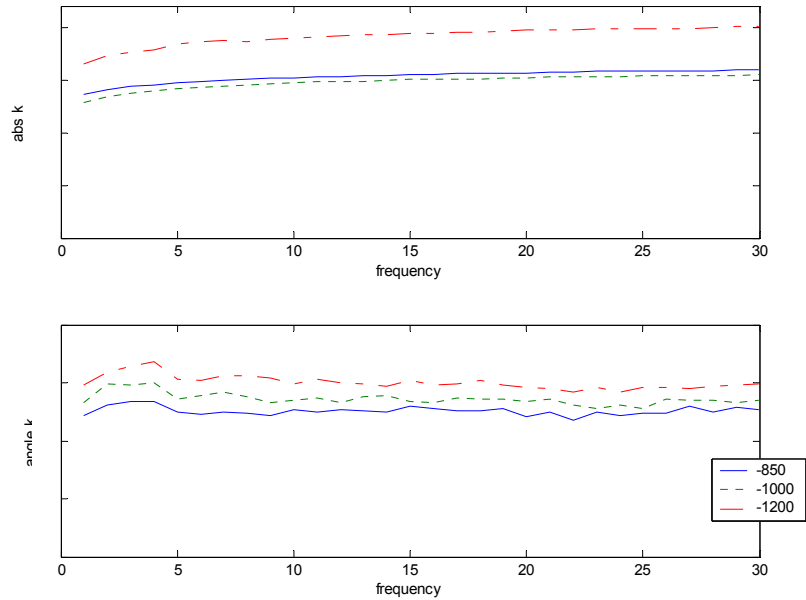


Figure 15: Measured dynamic stiffness and phase angle for 1 mm amplitude excitation; closed orifice configuration

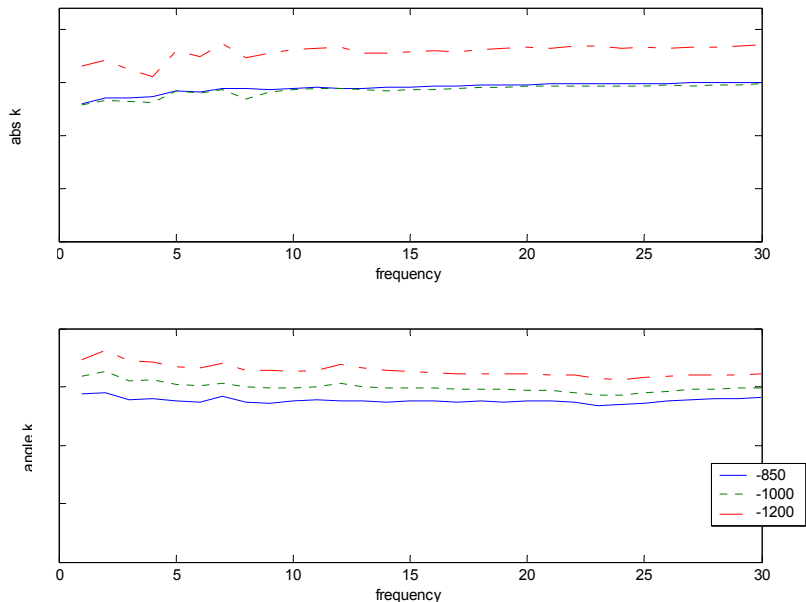


Figure 16: Measured dynamic stiffness and phase angle for 0.1 mm amplitude excitation; closed orifice configuration

Out of those results (figures 15 and 16), one gets the dynamic stiffness contribution of the air chamber and the rubber. This measurement gives the upper limit of the dynamic stiffness of the mount.

What can also be remarked, is that the stiffness for  $-1200$  N preload is larger than for the other two preloads. In fact, the air volume effect is here seen and at  $-1200$  N the working chamber volume is



much smaller than for the other preloads and the change of pressure over the change of volume is much higher. That is why the stiffness is larger for  $-1200$  N preload.

### 5. The pneumatic engine mount with opened orifice

The orifice is opened in order to be 20 mm diameter. Then the dynamic stiffness measurements are done again.

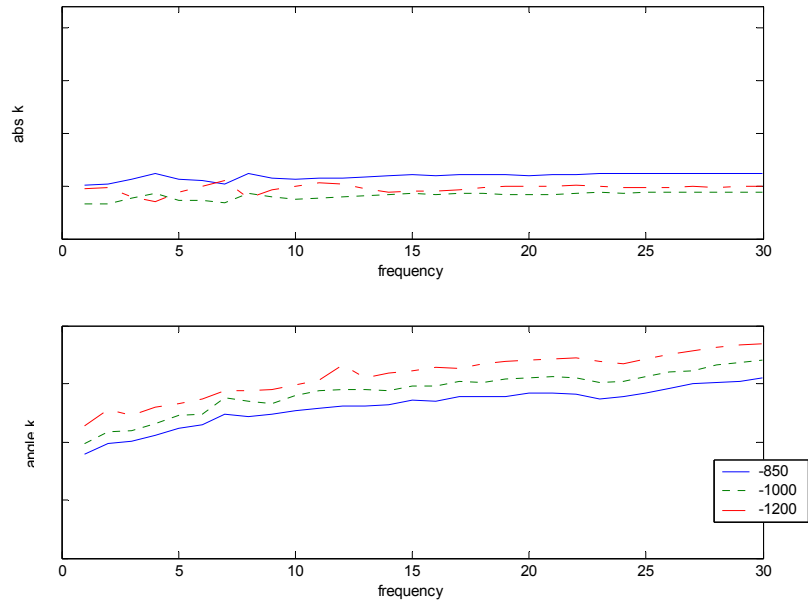


Figure 17: Measured dynamic stiffness and phase angle for 1 mm amplitude excitation; opened orifice configuration

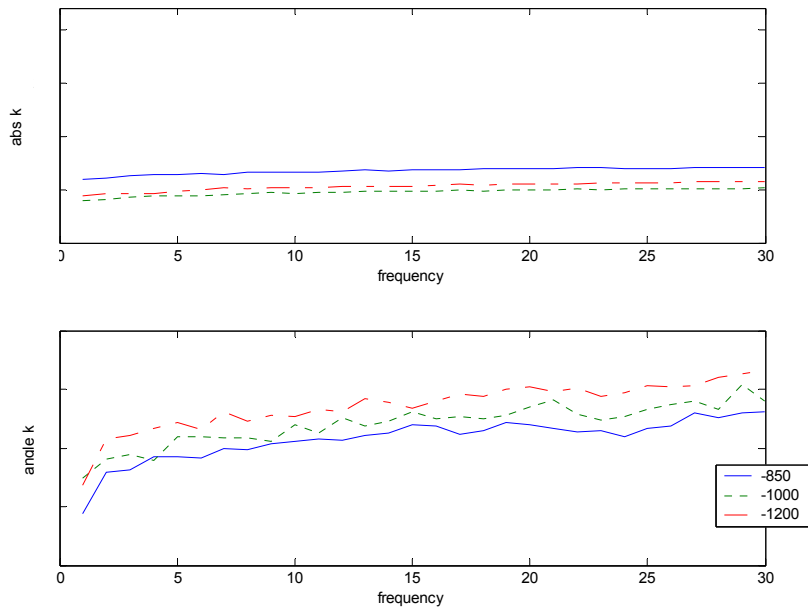


Figure 18: Measured dynamic stiffness and phase angle for 0.1 mm amplitude excitation; opened orifice configuration

Out of those results (curves 17 and 18), one gets the rubber dynamic properties in the proper geometry: the elastic stiffness and phase angle. In fact, the air is not playing any role in this configuration since the air volume is seen as infinite since the orifice is big: the air stiffness is much lower than the rubber stiffness. In this case, the total mount stiffness for  $-850$  N preload is the highest because the slope of the force deflection curve, which gives the static stiffness of the mount, is decreasing then increasing slightly (see figure 10).

## VIII. Description of the model

In this part will be derived the equation of the total dynamic complex stiffness of the pneumatic engine mount, which will be used to implement the model of the pneumatic engine mount with MATLAB.

### 1. Unknowns and assumptions

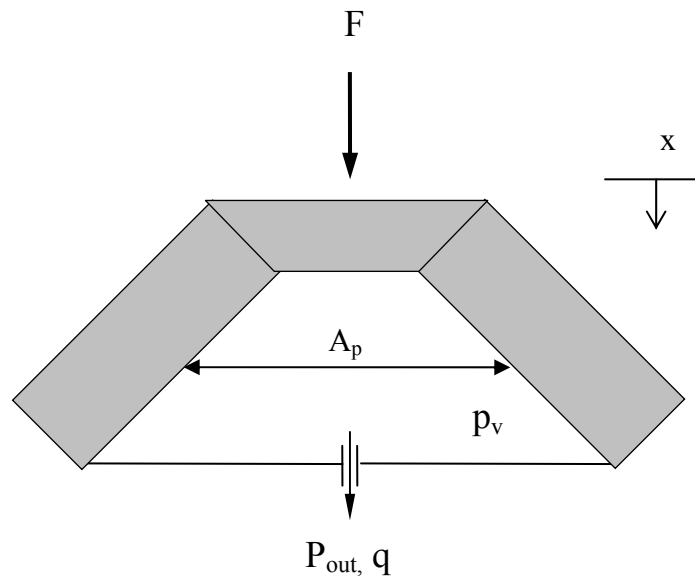


Figure 19: mount schema

$A_p$	Piston area, [m <sup>2</sup> ]
$C_{air}$	Air compliance, [m <sup>5</sup> /N]
$d_r$	Rubber viscous damping, [N/(m.s)]
$F$	Excitation force, [N]
$\ell$	Thickness of the plate (length of the orifice), [m]
$P_{out}$	Pressure at the output of the hole, [Pa]
$P_v$	Chamber pressure, [Pa]
$q$	Air flow through the hole, [m <sup>3</sup> /s]
$r$	Radius of the orifice, [m]
$S$	Steel plate area, [m <sup>2</sup> ]
$V$	Chamber volume, [m <sup>3</sup> ]
$x_e$	Displacement amplitude, [m]
$Z_i$	Inner impedance of the hole, [Ns/m <sup>5</sup> ]
$Z_r$	Radiation impedance of the hole, [Ns/m <sup>5</sup> ]
$\delta$	Rubber loss angle, [°]
$\kappa_{air+hole}$	Orifice and air stiffness contribution, [N/m]
$\kappa_r$	Rubber linear stiffness, [N/m]
$\kappa_{rtot}$	Complex rubber stiffness, [N/m]
$\kappa_{tot}$	Total mount stiffness, [N/m]

The different parts of the model to take into account are:

- The rubber, which is modelled with Voigt model.
- The hole, which is modelled has having an inner impedance and an output impedance. Those impedances are both defined in chapter VI.
- The air volume, which is modelled has having a stiffness of a pneumatic spring as in chapter IV.

The unknowns of the model are:  $P_v$ ,  $P_{out}$ ,  $q$ .

It is assumed that:

- The density of the gas in the chamber is constant in space and time
- The equations are transformed into Laplace domain to get the transfer complex stiffness

### 2. The air compliance expression

The air compliance  $\kappa_{air}$  is computed as a closed volume compliance, which is the same as in the paragraph 2 of chapter IV.

$$\kappa_{air} = \frac{\gamma P_{in} A_p^2}{V_0} \left[ \frac{1}{1 - \left( \frac{A_p}{V_0} \right) x_e} \right]^{(\gamma+1)} \quad (10.1)$$

### 3. The rubber model used

The rubber is modelled with Voigt model. For this model the rubber is taken has having a linear stiffness  $\kappa_r$  and a viscous damping  $d_r$ .

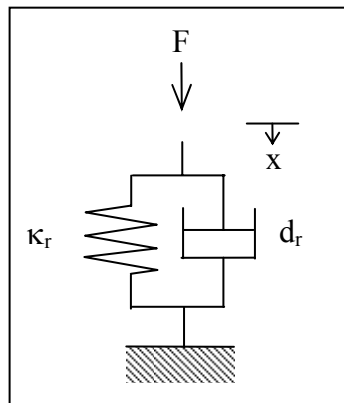


Figure 20: Voigt model of rubber element

The differential equation is then:  $d_r \dot{x} + \kappa_r x = f$ , and in frequency domain:  $(j\omega d_r + \kappa_r)X = F$

The loss angle of the rubber is defined as:  $\tan(\delta) = \frac{\omega d_r}{\kappa_r}$  and finally:

$$\kappa_{\text{tot}} = \kappa_r (1 + j \cdot \tan(\delta)) \quad (10.2)$$

#### 4. The basic equations used for the fluid

The equations concerning the air are:

$$\text{The force equilibrium of the air: } F(t) = Sp_v(t) \quad (10.3)$$

$$\text{The continuity equation in term of air compliance: } p_v(t) = \frac{\Delta V}{C_{\text{air}}}, \quad C_{\text{air}} = \frac{A_p^2}{\kappa_{\text{air}}} \quad (10.4)$$

$$\text{The volume conservation: } \Delta V = A_p x_e - \Delta x_i A_t \quad (10.5)$$

The equation concerning the hole:

$$\text{The driving flow through the hole: } p_v(t) - p_{\text{out}}(t) = Z_i q_t(t) \quad (10.6)$$

$$\text{The definition of the radiation impedance of the hole: } p_{\text{out}}(t) = Z_s q_t(t) \quad (10.7)$$

$\kappa_{\text{air}}$  is the air compliance as defined in equation (10.1).  $Z_i$  and  $Z_s$  are defined in chapter VII.  
Then:

$$\Delta V = \left[ A_p x_e + \frac{p_v}{j\omega(Z_i + Z_s)} \right]$$

$$p_v = \frac{\Delta V}{C_{\text{air}}} = \left[ A_p x_e - \frac{p_v}{j\omega(Z_i + Z_s)} \right] \frac{1}{C_{\text{air}}}$$

$$p_v = \frac{A_p x_e / C_{\text{air}}}{\left[ 1 + \frac{1}{j\omega(Z_i + Z_s)C_{\text{air}}} \right]}$$

$$\text{Finally: } \kappa_{\text{air+hole}} = \frac{F}{x_e} = \frac{SA_p / C_{\text{air}}}{\left[ 1 + \frac{1}{j\omega(Z_i + Z_s)C_{\text{air}}} \right]} \quad (10.8)$$

Since the air and the rubber spring are playing in parallel, the total complex stiffness is:

$$\kappa_{\text{tot}} = \kappa_{\text{air+hole}} + \kappa_{\text{tot}} = \frac{SA_p / C_{\text{air}}}{\left[ 1 + \frac{1}{j\omega(Z_i + Z_s)C_{\text{air}}} \right]} + \kappa_r (1 + j \cdot \tan(\delta)) \quad (10.9)$$

Then, the term  $\kappa_{\text{air+orifice}}$  can be written as:  $\frac{(SA_p)^2 j\omega(Z_i + Z_s)/C_{\text{air}}}{SA_p j\omega(Z_i + Z_s) + SA_p/C_{\text{air}}}$ . If  $Z_s$  is neglected and  $Z_i$  expressed as in equation (7.6), on gets the equation (7.8)

$$\kappa_{\text{air+hole}} = \frac{(SA_p)^2 j\omega(Z_i + Z_s)/C_{\text{air}}}{SA_p j\omega(Z_i + Z_s) + SA_p/C_{\text{air}}} = \frac{(SA_p)^2 j\omega \left( j\omega\rho + \frac{2\mu\beta}{r}(1+j) \right) \frac{\ell}{A_p} / C_{\text{air}}}{SA_p j\omega \left( j\omega\rho + \frac{2\mu\beta}{r}(1+j) \right) \frac{\ell}{A_p} + SA_p/C_{\text{air}}} \quad (7.8)$$

$$\text{Finally: } \kappa_{\text{air+hole}} = \frac{S\ell \left( (j\omega)^2 \rho + \frac{2\mu\beta}{r} j\omega(1+j) \right) \cdot SA_p / C_{\text{air}}}{S\ell \left( (j\omega)^2 \rho + \frac{2\mu\beta}{r} j\omega(1+j) \right) + SA_p / C_{\text{air}}}$$

The air volume is modelled as a spring with a stiffness  $\kappa_{\text{air-model}} = SA_p/C_{\text{air}}$  and the orifice is modelled as a mass  $m_{\text{orifice}} = \rho S\ell$  in parallel with a dashpot  $d_{\text{orifice}} = \frac{2\mu\beta}{r}(1+j)$ . The air volume and orifice are acting in serie. The analogous mechanical system is in figure 21.

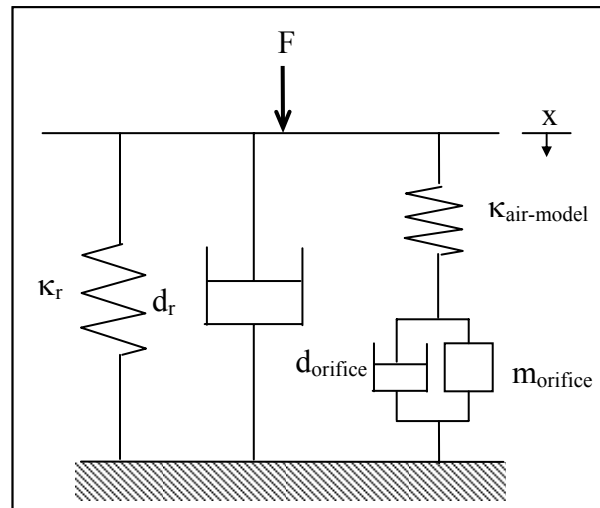


Figure 21: pneumatic mount model analogous mechanical system

The mass  $m_{\text{orifice}}$  corresponds to the mass of air in the orifice  $d_{\text{orifice}}$  corresponds to the losses in the hole due to shear forces.

### 5. The limits of the model

The upper limit is given by the rubber stiffness together with the air stiffness for closed volume and the lower limit is given by the rubber stiffness only, as pointed out with the measurements.

### 6. Numerical implementation in MATLAB

In the inner impedance non linear term  $0.5 \frac{\rho|v|}{A}$  (equation (7.7)), the particle velocity  $v$  has to be first calculated as  $v = \omega x_e$  as a rough approximation (this formula is true for compressible fluid).

This expression will be updated as:  $v = \frac{j\omega x_e S / A_t}{1 + C_{air}(Z_i + Z_s)}$ . The last formula comes from equation (10.6).

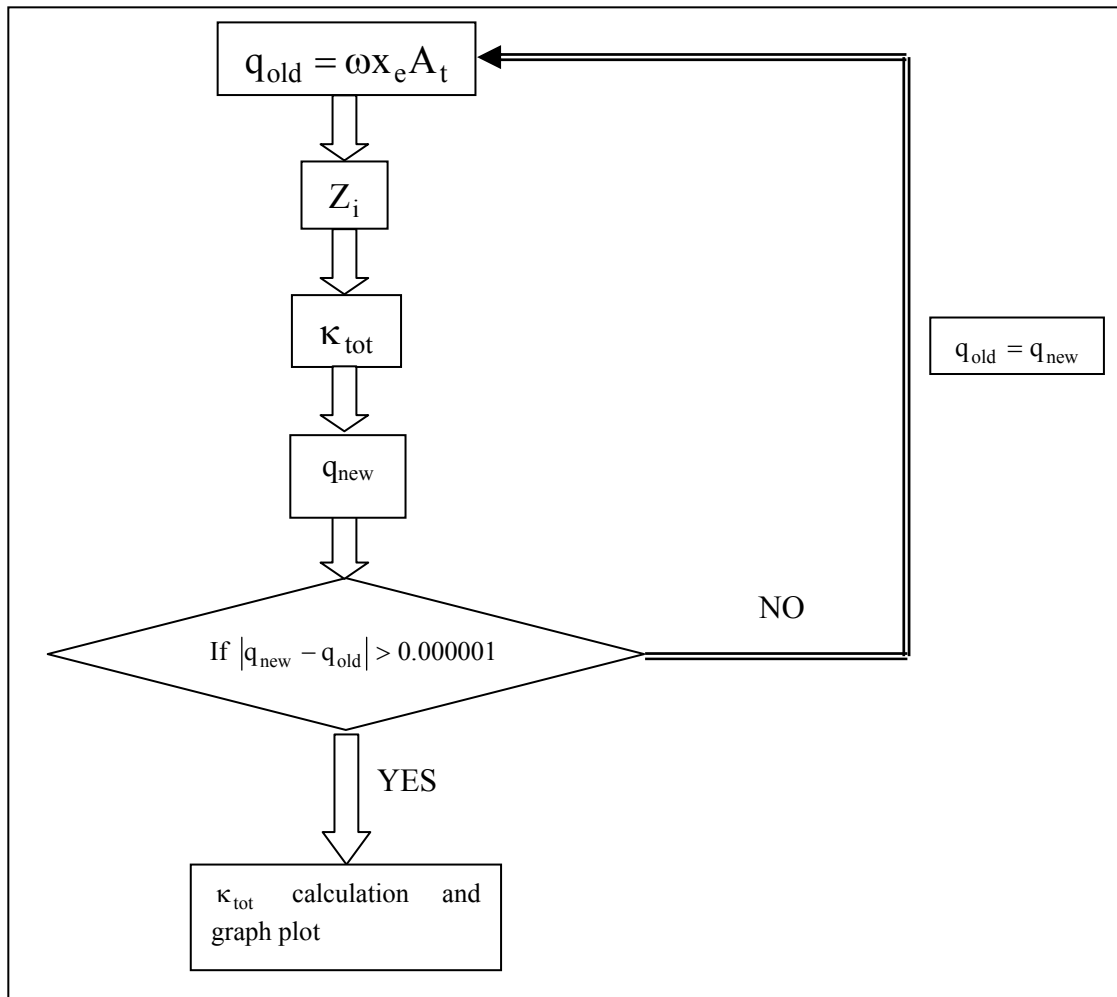


Figure 22: Program functionment chart

The volume and the pneumatic diameter are calculated with finite element method for the different preload. The preload influence is taken into account through the initial volume and the pneumatic diameter.

### 7. Parameter study

A parameter study in which the absolute value and the phase angle of the stiffness have been plotted in the same graph for a variation of  $\pm 10\%$  of each parameter has been done (see appendix B). The parameters are: the length of the hole, the diameter of the hole, the pneumatic diameter, the chamber volume, the steal plate diameter, the rubber stiffness and phase angle.

The conclusions of it are that:

- The diameter of the orifice gives the resonance frequency and can be adapted to tune the mount.
- The air chamber volume should be decreased in order to increase the damping. It also determines the behavior at the highest frequencies.
- The pneumatic diameter and the diameter of the steel plate below should be increased in order to increase the damping. As the volume, it also determines the dynamic stiffness at the highest frequencies.
- The rubber elastic stiffness should be as low as possible to get the highest damping.

This confirms the theory used and that the model is working in a proper way.

# IX. Model/measurements comparison

## 1. The rubber measurement and model comparison

From the Voigt model, the rubber absolute stiffness and phase angle are taken as constant values, which could be chosen as the average of the measured absolute stiffness and phase angle with opened orifice configuration. In that case, the curves are good only after about 10 Hz. In fact, it is hard to model the dynamic properties of the rubber at low frequencies. But those values can also be taken from the measurements with opened hole, and then as frequency dependent. In this case, the curves are fitting with the measured one in the entire frequency range.

In the figure 23 are the comparison between the calculated curves with the rubber properties taken as constant and the calculated curves with measured rubber properties.

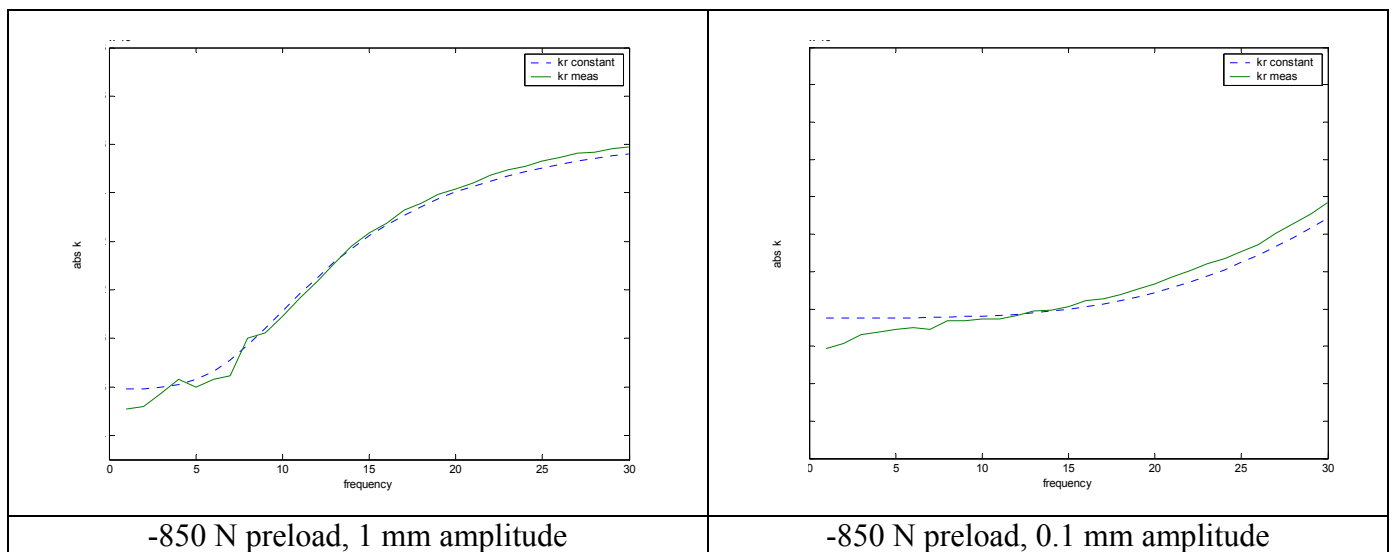


Figure 23: Comparison between different rubber properties calculation

## 2. Measurements and model fit

In looking at the parameter study, the relevant parameters that could be tuned are:

- The pneumatic diameter
- The volume
- The rubber elastic stiffness
- The rubber phase angle.

In fact, the diameter of the orifice is only shifting the resonance frequency of the system, which the model gives correctly and there is no reason that the steel plate diameter should be wrong. Anyway, since the influence of this parameter is the same as the pneumatic diameter, if there is any uncertainty, it would be contained in the pneumatic diameter factor. In the appendix C are plotted the stiffness and phase angle of the mount: in the same figure, the calculated (calc) and measured (meas) curves can be seen.

Regarding the curves comparison without factor, it can be seen that the stiffness for 1 Hz are not matching. This should be the case because at low frequencies, the air movement is so low that the behavior of the mount is similar to the static case and only the elastic stiffness of the rubber is seen. But this could be explained by the fact that for the calculates curves, the rubber stiffness is taken from the opened orifice measurements, which gives a slightly different rubber elastic stiffness than



in the normal dynamic measurements: the rubber properties are changing with the time and are sensible to fatigue. Then, if the calculated curves are shifted to the same start stiffness value as the measured one, the calculated absolute value of the stiffness is getting higher than the measured one for higher frequencies. The phenomenon is the same for the phase angle. It can be concluded that the calculated air stiffness is too high, which is confirmed by the fact that the volume has to be multiplied by a factor almost two in order to get a good fit between the measured and calculated curves (the total mount stiffness is depending on the volume only via the air volume stiffness. There are only some clues to explain this:

- The volume is really small and some unknown phenomena could happen.
- The air stiffness is calculated for a squared box geometry: the geometry of the rubber part of the mount is not taken into account and could play a role
- There could be some measurements uncertainty.

## X. Proposals how to increase the damping

### 1. Several holes, orifice area increase

With the model, it could be shown that having several small holes (smaller than the one taken so far), increases slightly the damping. In the same graph are plotted the absolute value and the phase angle of the complex stiffness for different areas:

- The first area is the normal orifice area corresponding to a circular orifice of 2 mm diameter
- The second area correspond to two circular orifices of 2 mm diameter
- The third area correspond to two orifices of 1 mm diameter
- The fourth area correspond to four orifices of  $1/\sqrt{2}$  mm diameter

The first, third and fourth case corresponds to a same total area.

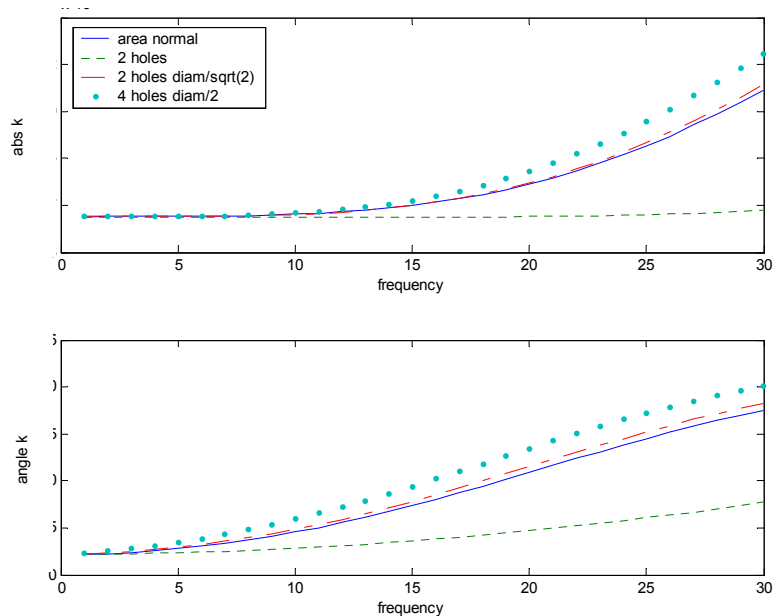


Figure 22: Computed dynamic stiffness and phase angle for 0.1 mm amplitude excitation; different orifice configurations

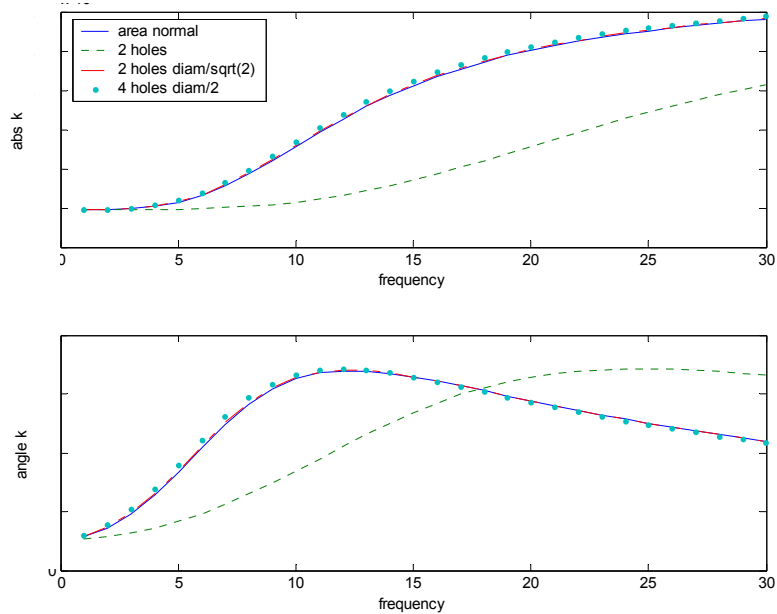


Figure 23: Computed dynamic stiffness and phase angle for 1 mm amplitude excitation; different orifice configurations

Then it can be seen that increasing the total area is shifting the resonance frequency as pointed in the parameter study, but for a same area distributed on several holes, the damping is almost not increasing and since it would anyway be too complicated to make it industrially, no measurements has been done to verify those results.

## 2. Acoustic absorbent inside the volume

L. Beranek in Ref [5] is discussing the influence of absorptive lining in loudspeaker closed box. A conclusion is that the absorber makes the speed of sound decreasing in the box because the compression becomes isothermal. Then, the ratio of specific heats decreases from 1.4 to 1, which means that the air compliance is increasing.

Since it is difficult to get the absorber acoustical properties, it hasn't been tried to include them in the model.

## XI. Conclusion and discussion

After having understood how an hydraulic mount is working and explored some simple pneumatic spring, the model of the pneumatic mount has been implemented in MATLAB and finally, the calculated curves are compared to the measured one. The mount has physically been divided in three parts in order to model it more easily and the conclusion of the model-experiment study shows that:

- The rubber part is well modelled with a spring in parallel with a dashpot,
- The orifice impedances seems to be quite correctly modelled since the global model predicts really well the resonance frequency; in fact, the channel geometry and behavior determine the frequency of maximum phase angle and the damping properties.
- The air compliance is not modelled accurately enough since the calculated phase angle is always too high compared to the measured one.

It can be also remarked that the simplified orifice impedance is working well for the chosen frequency range and for this application.

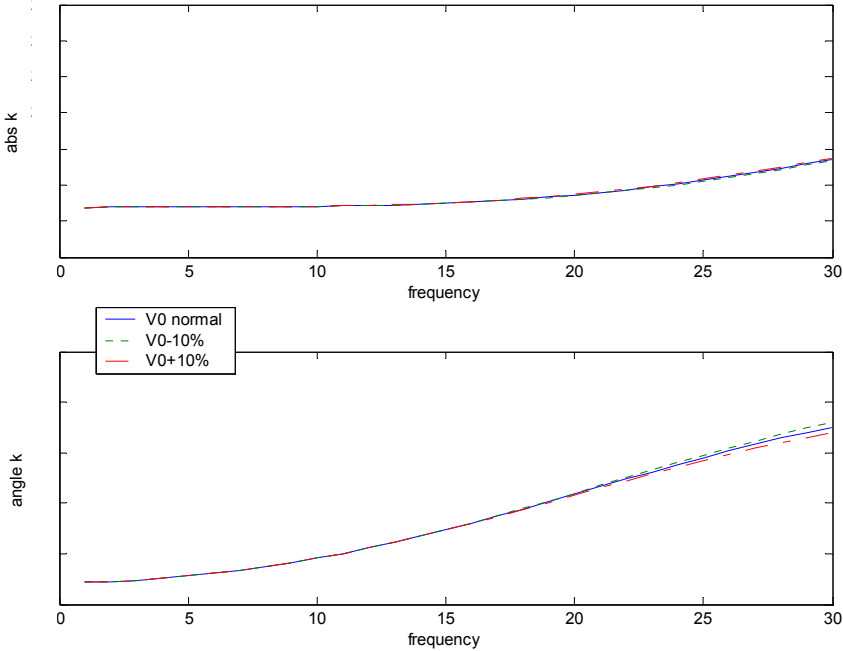
Then, the next step to do in order to improve the model would be to find a better air stiffness approximation: the total mount stiffness at the highest frequencies would be better modelled. For that, the air stiffness model should include the mount geometry. Finally, a non-linear model for large amplitudes with small air cavity volume could be useful to get a modelisation in time domain.

## REFERENCES

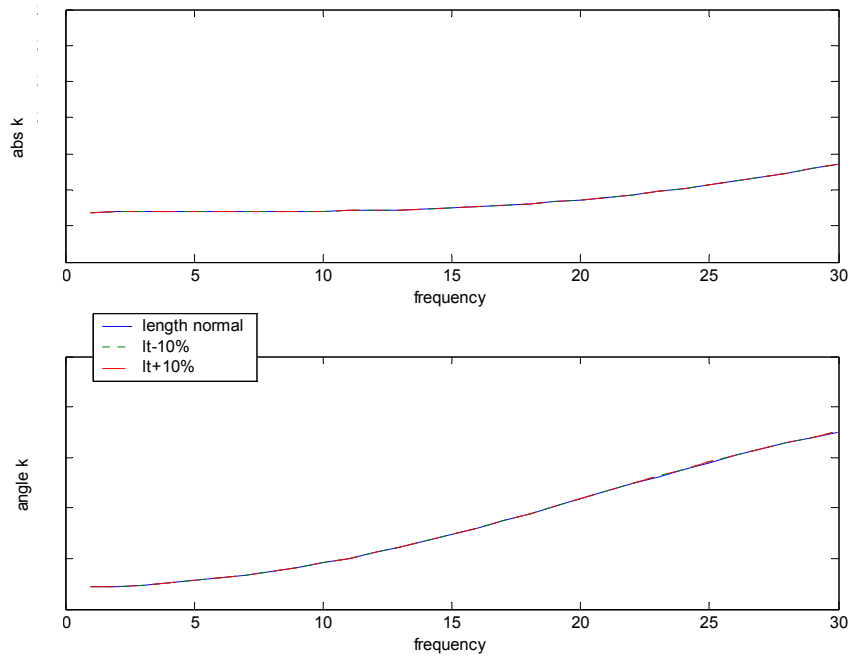
1. J. E. COLGATE, C.-T. CHANG, Y.-C. CHIOU, W. K. LIU AND L. M. KEER 1995. *Modelling of a hydraulic engine mount focusing on response to sinusoidal and composite excitations*, Journal of Sound and Vibration, 184:503-528.
2. R. SINGH, G. KIM AND P. V. RAVINDRA 1992. *Linear analysis of automotive hydro-mechanical mount with emphasis on decoupler characteristics*, Journal of Sound and Vibration, 158:219-243.
3. SHI-JIAN ZHU, XUE-TAO WENG, GANG CHEN 2003. *Modelling of the stiffness of elastic body*, Journal of Sound and Vibration, 262:1-9.
4. CLARENCE W. DE SILVA 1999. *Vibration: fundamental and practice*, CRC press.
5. LEO L. BERANEK 1954. *Acoustics*, Mac Graw Hill, New-York.
6. J.A. FOX 1974. *An introduction to engineering fluid mechanics*.
7. EUGENE I. RIVIN 2003. *Passive Vibration Isolation*, ASME press.
8. M. SORLI, L. GASTALDI, E. CODINA, S. DE LAS HERAS 1999. *Dynamic analysis of pneumatic actuators*, Simulation Practice and Theory 7, 589-602.
9. W.M.BELTMAN 1998. *Viscothermal wave propagation including acousto-elastic interaction*, PhD thesis, University of Twente, The Netherland.
10. M. HOFMANN 2002. *Antivibration systems*.
11. A. GEISBERGER, A. KHAJEPOUR AND F. GOLNARAGHI 2002. *Non-linear modelling of hydraulic mount: theory and experiment*, Journal of Sound and Vibration, 249:371-397.
12. L. J. SIVIAN 1935, *Acoustic impedance of small orifices*, Journal of the acoustical society of America, volume 7:94-101.
13. B. I. BACHRACH and E. RIVIN 1982, *Analysis of a damped pneumatic spring*, Journal of Sound and Vibration, 86(2):191-197.
14. RONALD M. AARTS and AUGUSTUS J. E. M. JANSSEN 2003, *Approximation of the struve function H occurring in impedance calculations*, Journal of the acoustical society of America, 113 (5): 2635-2637
15. IRVING B. CRANDALL 1927. *Theory of vibrating systems and sounds*, D. Van Nostrand Company, New-York.
16. *Engineering with Rubber*; edited by Alan N. GENT with contributions by R.P. CAMPION and others, University of Akron, USA

# XII. APPENDIX A1: Parameter study for -850 N preload and 0.1 mm amplitude

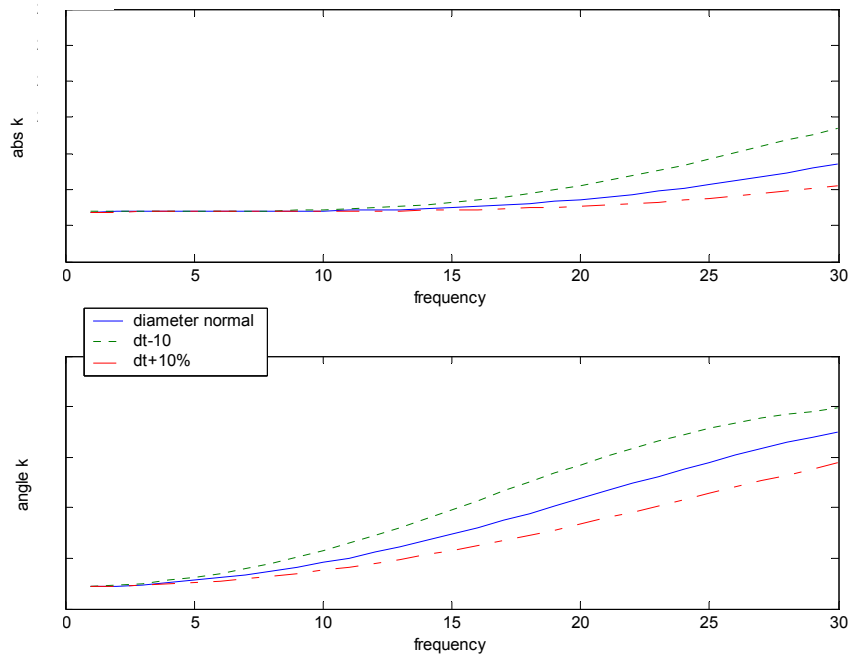
## Volume variation



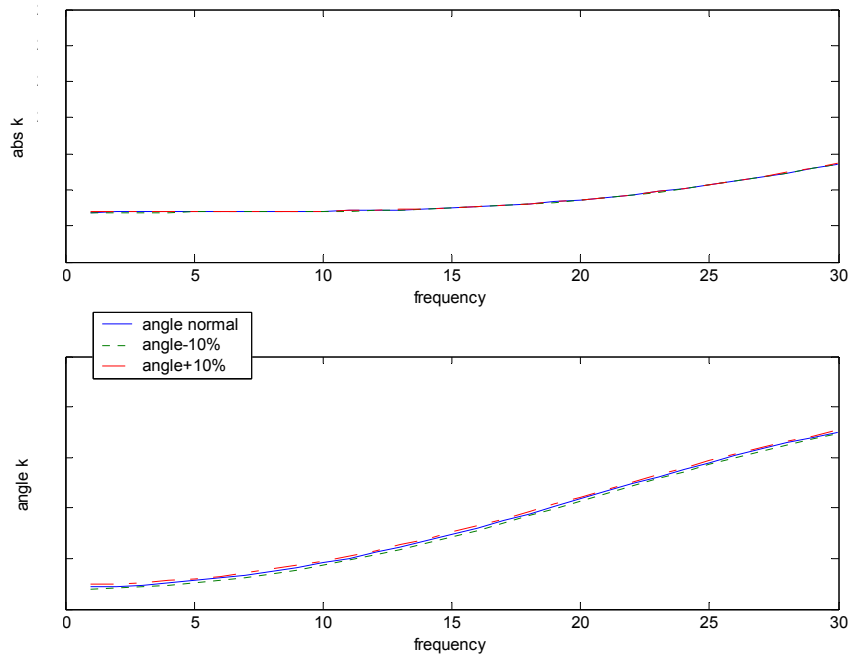
## Length of the orifice variation



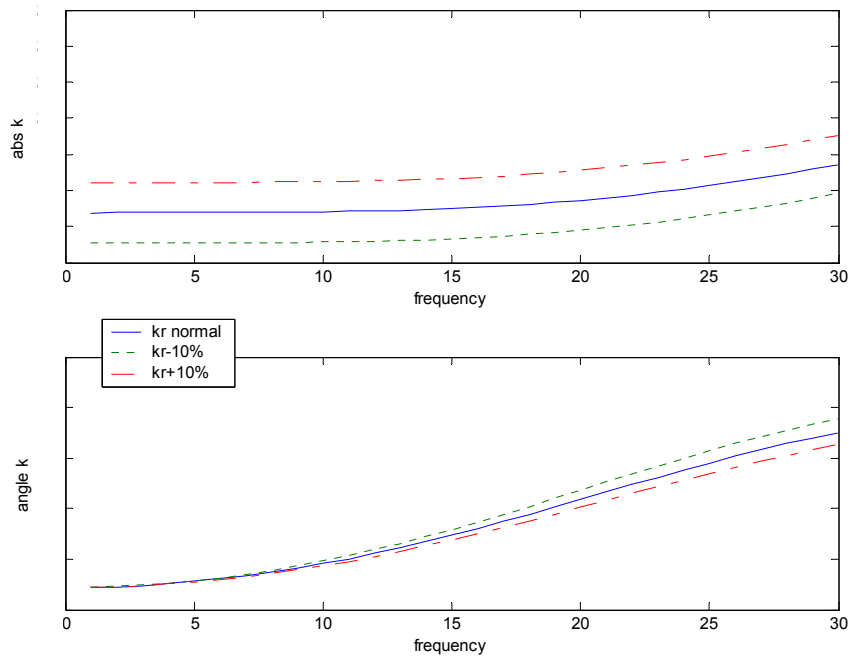
## Diameter of the orifice variation



## Angle of rubber damping variation

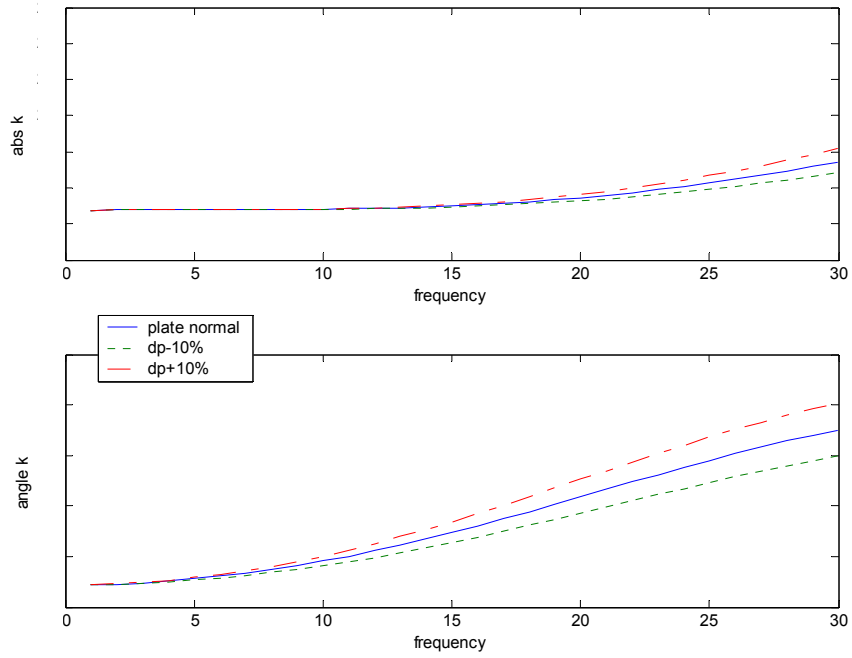


## Rubber elastic stiffness variation

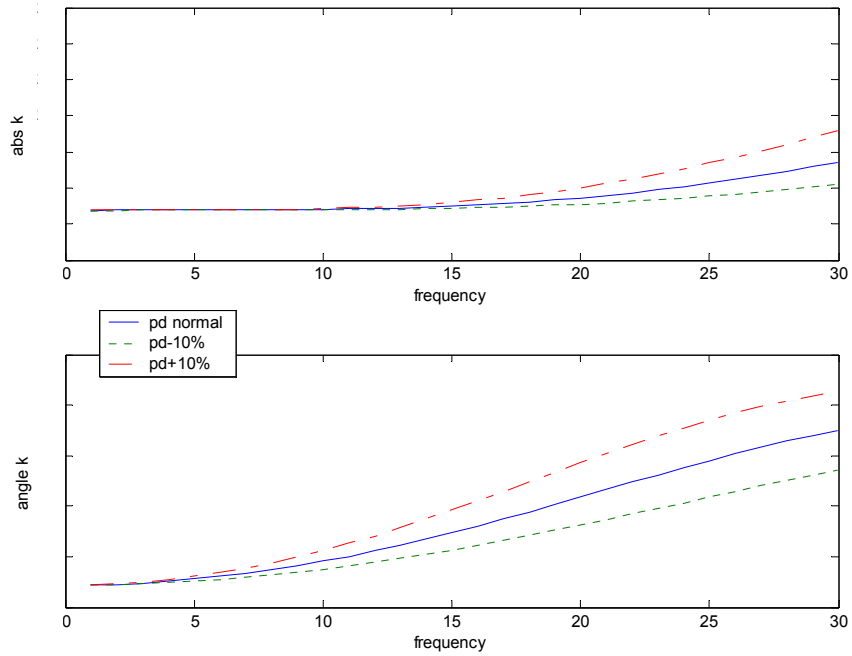




## Diameter of the plate below variation

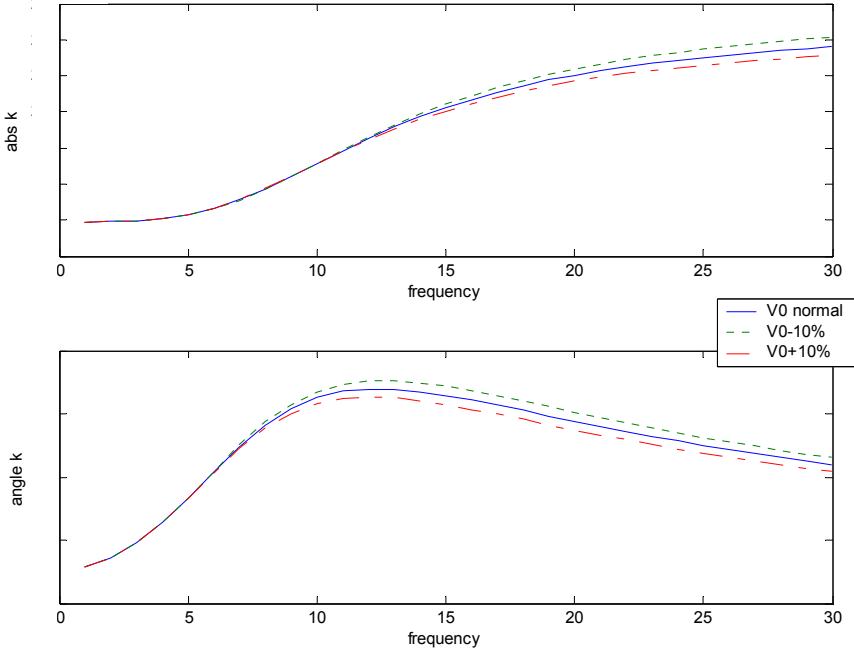


## Pneumatic diameter variation

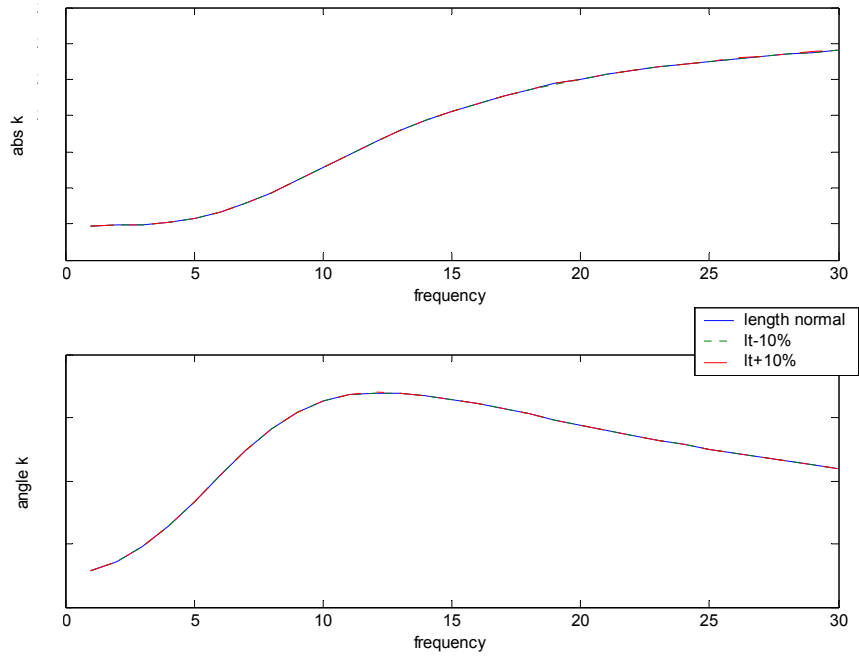


# XIII. APPENDIX A2: Parameter study for -850 N preload and 1 mm amplitude

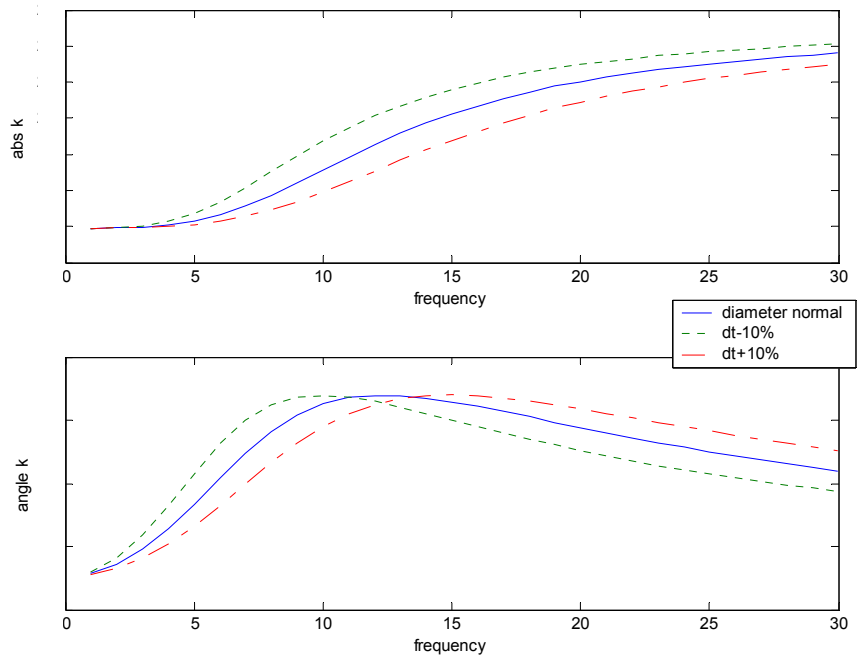
## Volume variation



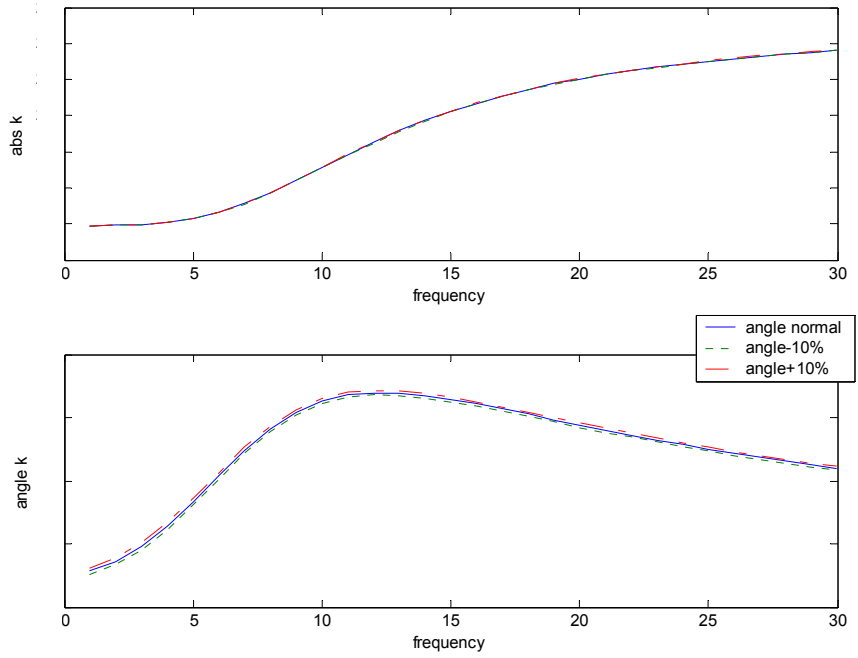
## Length of the orifice variation



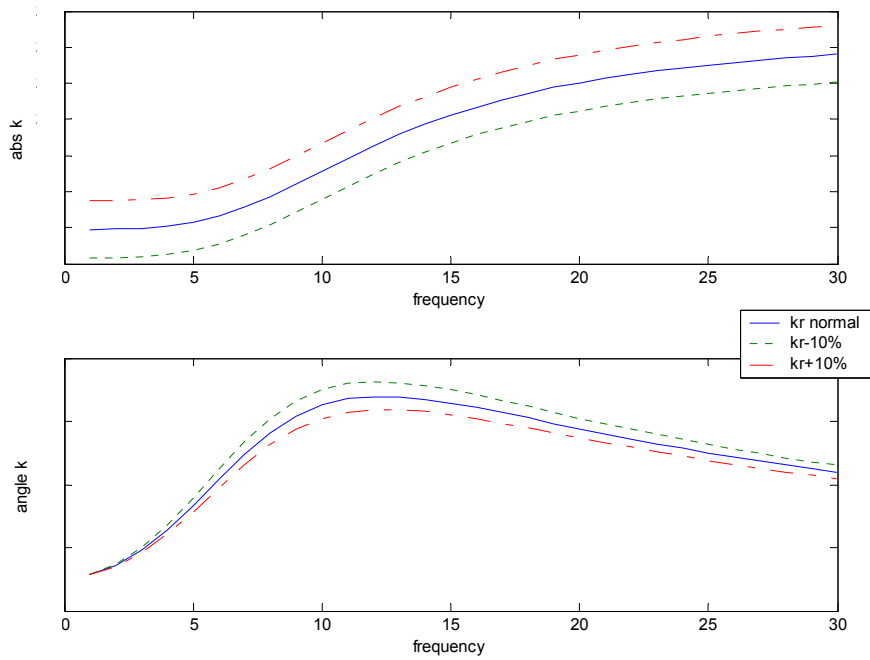
## Diameter of the orifice variation



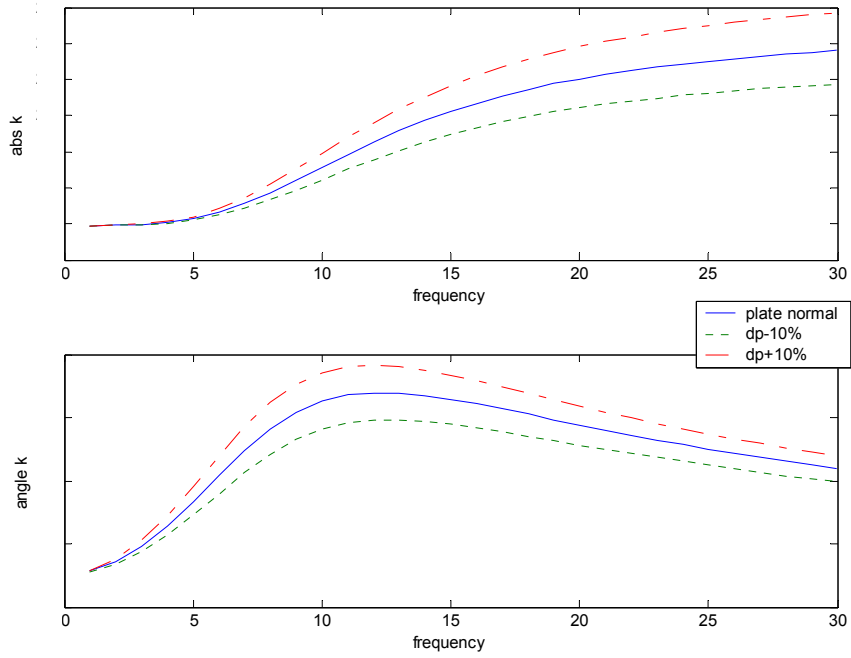
## Angle of rubber damping variation



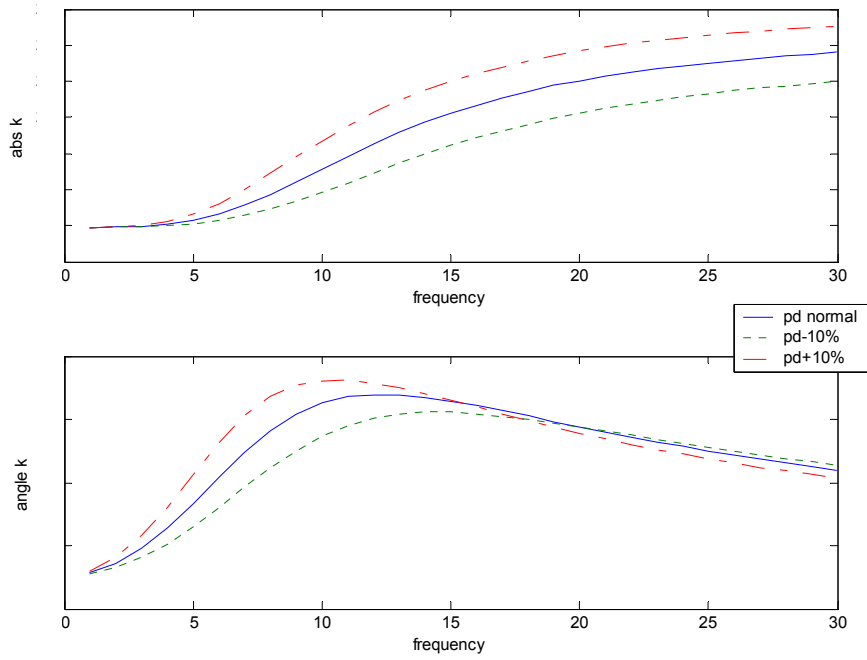
## Rubber elastic stiffness variation



## Diameter of the plate below variation

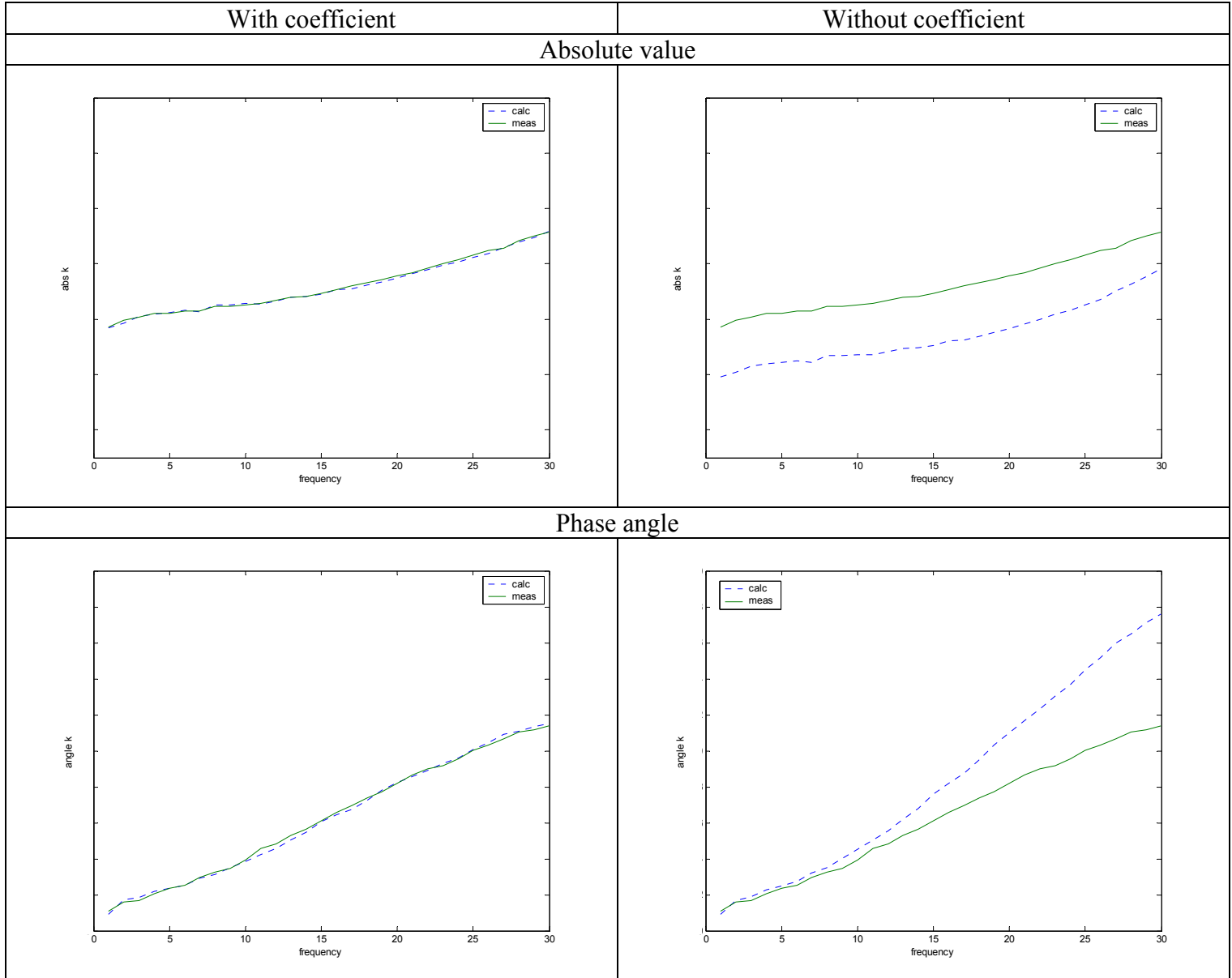


## Pneumatic diameter variation



# XIV. APPENDIX B: Calculated and measured curves comparison

-850 N preload, 0.1 mm amplitude

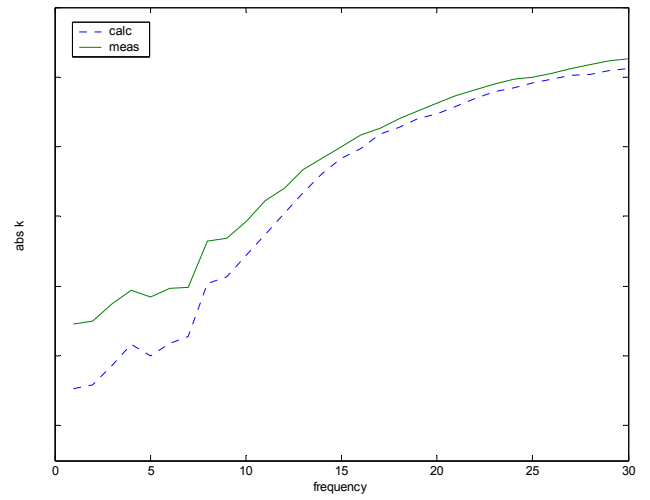
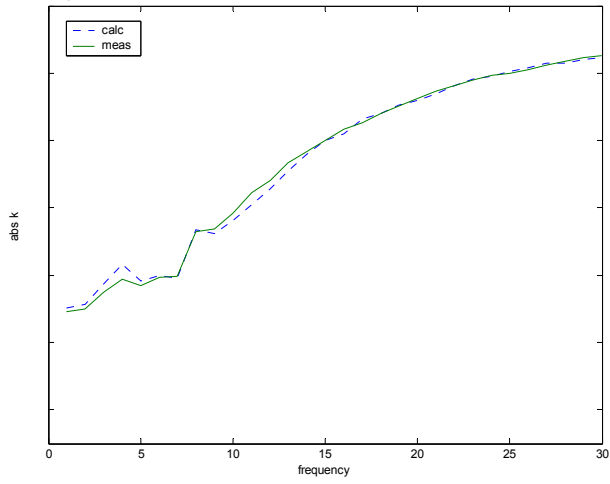


# -850 N preload, 1 mm amplitude

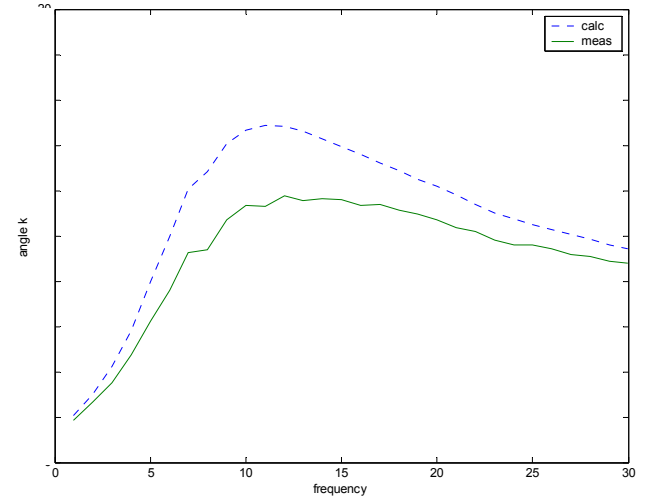
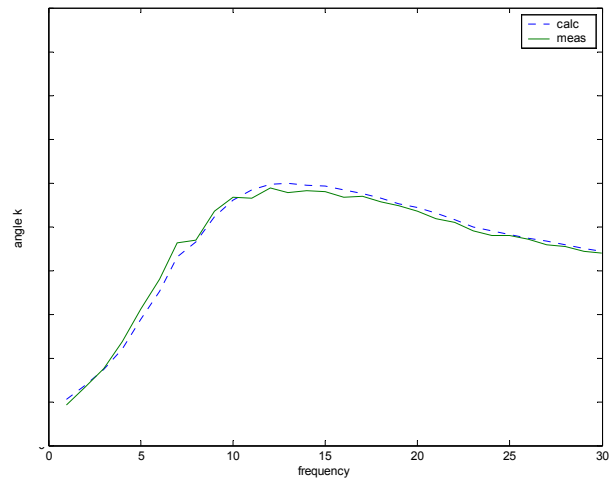
With coefficient

Without coefficient

Absolute value



Phase angle

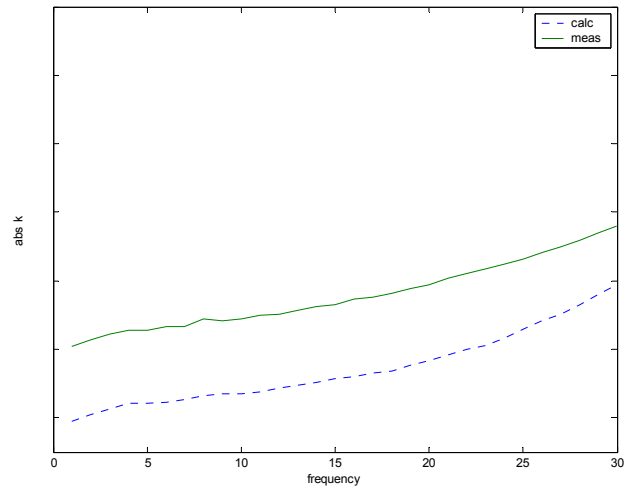
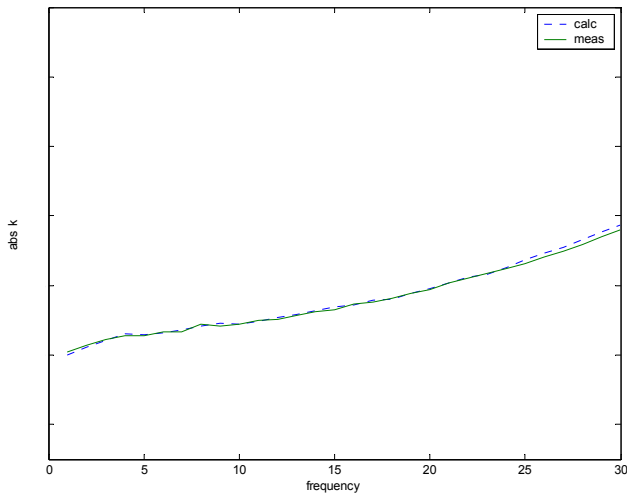


**-1000 N preload, 0.1 mm amplitude**

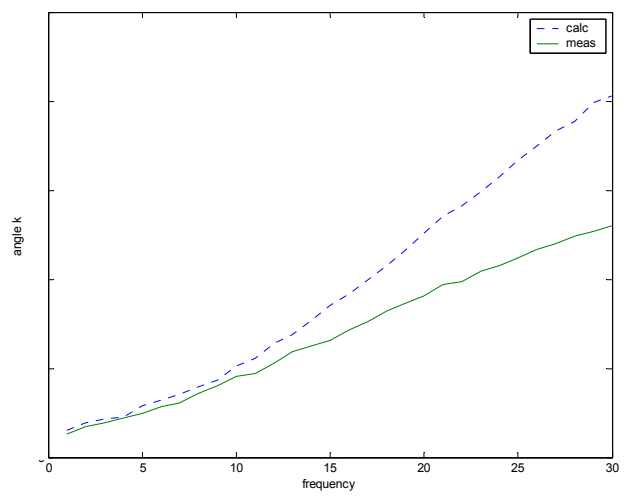
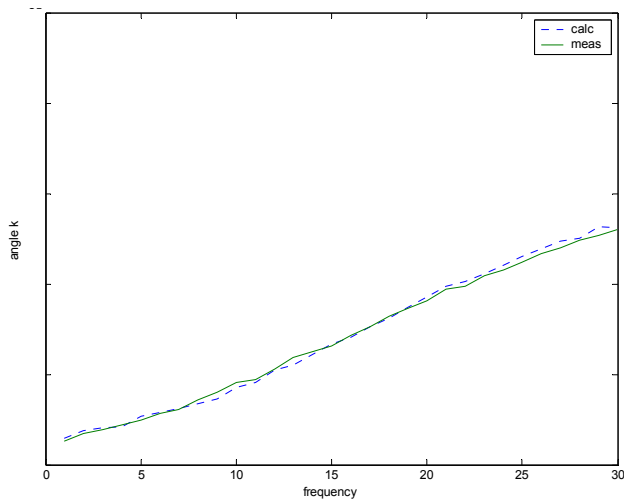
With coefficient

Without coefficient

Absolute value



Phase angle



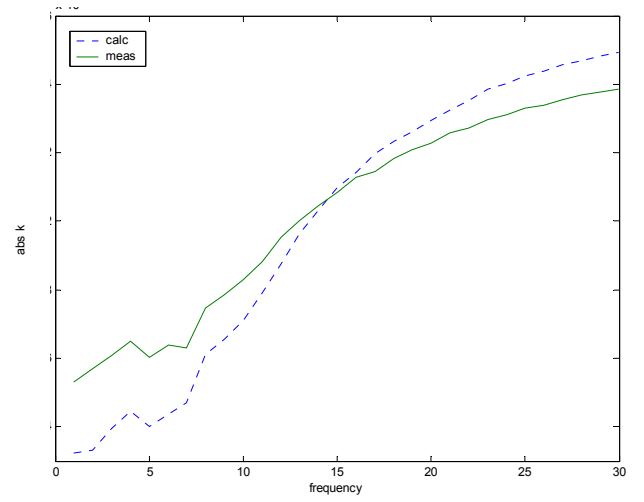
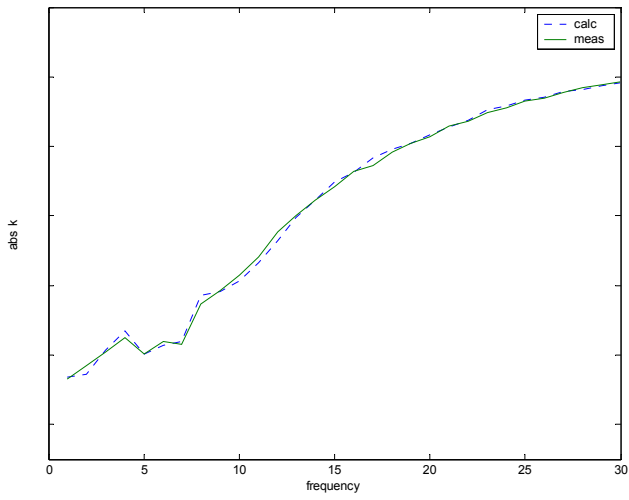


**-1000 N preload, 1 mm amplitude**

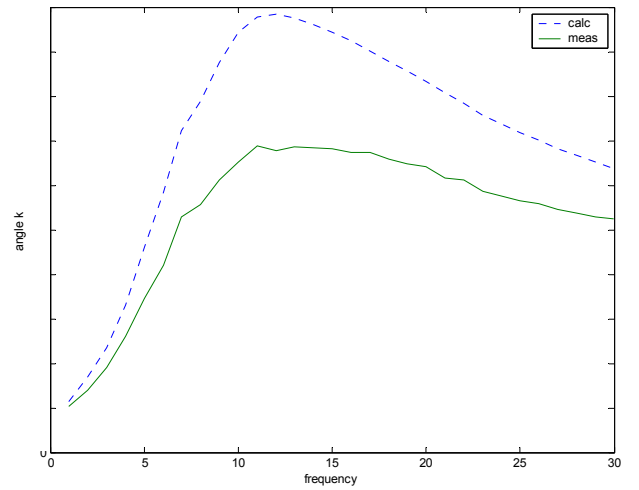
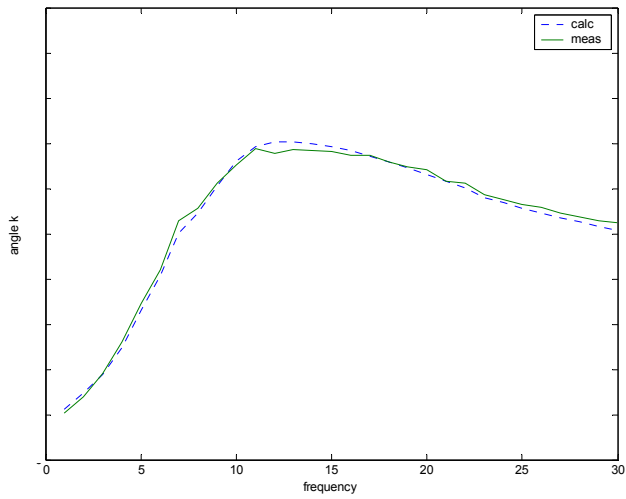
With coefficient

Without coefficient

Absolute value



Phase angle

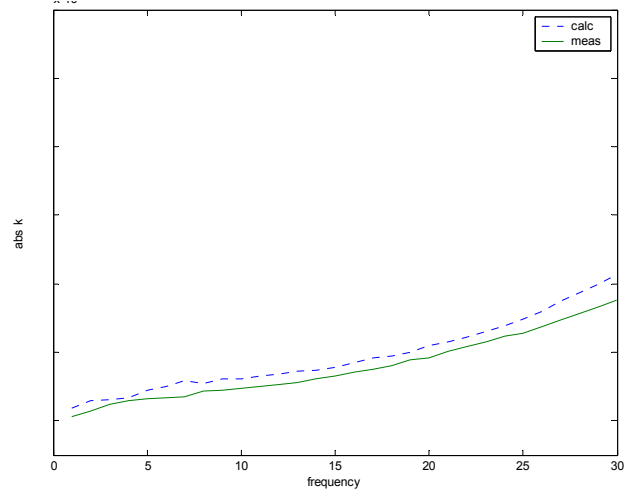
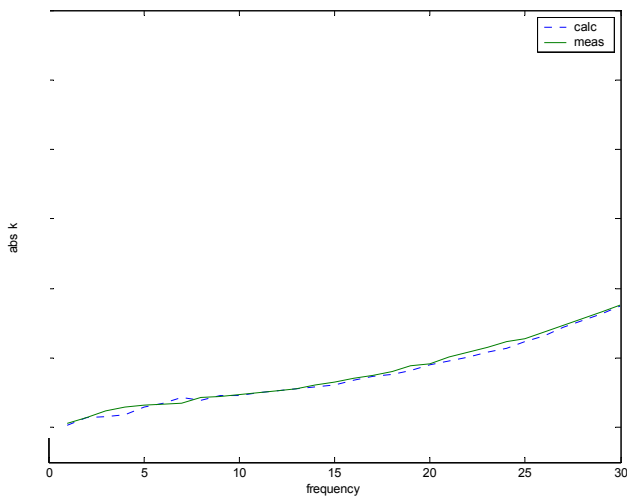


**-1200 N preload, 0.1 mm amplitude**

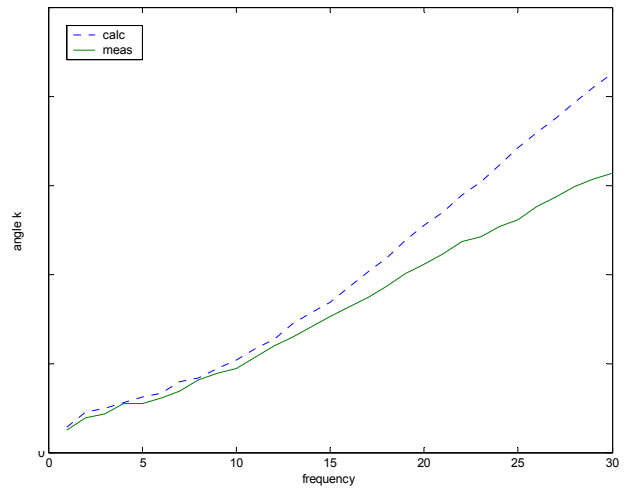
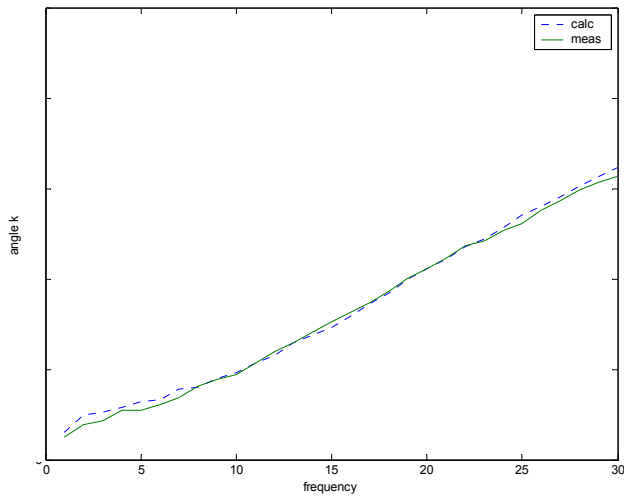
With coefficient

Without coefficient

Absolute value



Phase angle

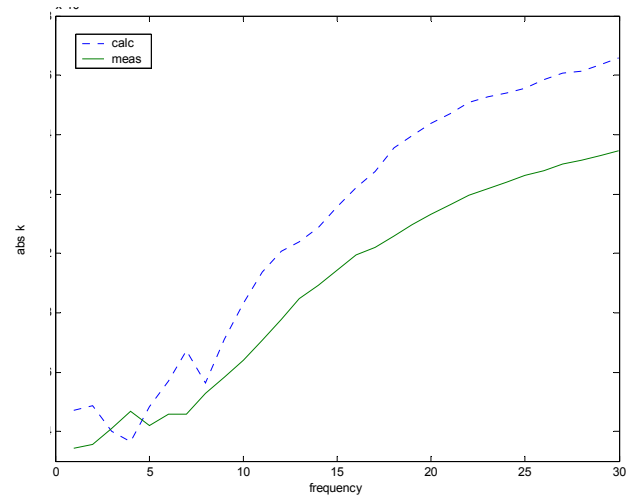
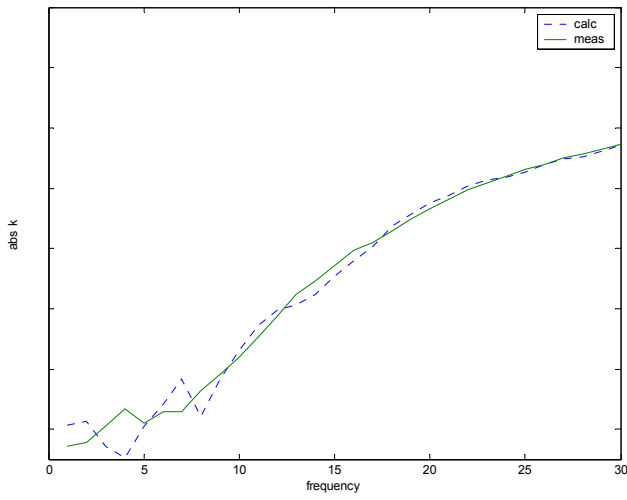


# -1200 N preload, 1mm amplitude

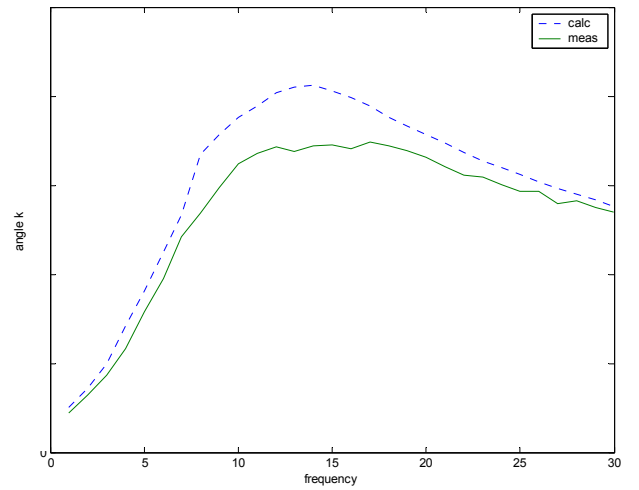
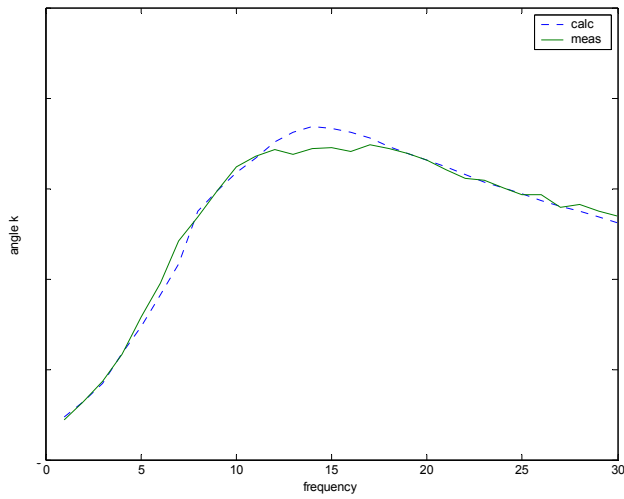
With coefficient

Without coefficient

Absolute value



Phase angle



## XV. APPENDIX C: MATLAB code

```
clear

%GEOMETRY

pd=0.08605; %pneumatic diameter m; -850 N
% pd=0.08622; %pneumatic diameter m; -1000 N
% pd=0.08619*0.93; %pneumatic diameter m; -1200 N

Ap=pi*(pd/2)^2; %piston area m^2

dt=0.002; %diameter of the hole m

r=dt/2; %radius of the hole m

At=pi*r^2; %cross section area of the hole m^2

dp=0.1017; %diameter of the plate below m

S=pi*(dp/2)^2 %area of the plate below m^2

lt=0.002; %length of the hole m

V0=38.4878*10^(-6); %initial volume m^3; -850 N
% V0=33.100*10^(-6); %initial volume m^3; -1000 N
% V0=25.627*10^(-6)*1.8; %initial volume m^3; -1200 N

%CONSTANTS

p0=101300 %atmospherique pressure Pa

rho=1.2255;%kg/m^3

gamma=1; %ratio of specific heats

kinvisc=17.98*10^(-6);%fluid dynamic viscosity (Pa.s)

c=343;%speed of sound in air m/s

%PARAMETERS

xe=0.001;%amplitude of the displacement

% xe=0.0001;%amplitude of the displacement

%AIR COMPLIANCE CALCULUS

aircomp=V0./(((1-Ap*xe/V0).^(gamma+1)).*(gamma*p0));
```

```

%VECTORS

omega=linspace(1,30,30)*2*pi;

s=j*omega;

ki=(omega.*rho./(2*kinvisc)).^(0.5);

k=omega./c;

wave=k.*r;

omegameas=linspace(1,30,30)*2*pi;

bessel_1=2./pi.*(((2.*wave).^3./3)-(2.*wave).^5./(3.^2.*5)+(2.*wave).^7./(3.^2.*5.^2.*7)-
(2.*wave).^9/(3.^2.*5.^2.*7^2*9)); %H1 serie

bessel_2=2./pi-besselj(0,2.*wave)+(16./pi-5).*(sin(2.*wave)/(2.*wave))+(12-36./pi).*(1-
cos(2.*wave))./(2.*wave).^2);

Zsunnorm=(rho.*c.*(pi.*r.^2)).*((1-besselj(1,2.*wave)/(wave))+j.*bessel_1./wave); % plane
piston in infinite baffle

Zs=Zsunnorm./((pi*r^2)^2);

Ziwf=(lt./(pi.*r.^2))*s.*rho.*(1./(1-(2./(ki.*r.*(-2*j)).^(0.5))).*besselj(1,ki.*r*(-
2*j)).^(0.5))./besselj(0,ki.*r.*(-2*j)).^(0.5))); %internal impedance of a small operture

for m=30:-1:1

err=1;

qiold(m)=xe*Ap*omega(m);

load measurefermeouvert

kr(m)=Kmeasferme2(m)*10^3*1.13*(1+j.*tan(pi*anglemeasferme2(m)*1.1/180));

    while err>0.000001

Zi(m)=Ziwf(m)+0.5*rho*abs(qiold(m))/At^2;

qi(m)=(xe*s(m)*Ap)/(1+((aircomp)*s(m)*(Zi(m)+Zs(m))));

K(m)=(S*Ap/(aircomp))/(1+1/(s(m)*(Zi(m)+Zs(m))*(aircomp)))+kr(m);

err=abs(qi(m)-qiold(m));

qiold(m)=qi(m);

    end

```

```
end

load measured_values_850_mine

figure(1)

plot(omega/(2*pi),abs(K),...
     omegameas/(2*pi),Kmeas2*10^3)

xlabel('frequency')

ylabel('abs k')

axis([0 30 1.3e5 3e5])

figure(2)

plot(omega/(2*pi),angle(K)*180/pi,...
     omegameas/(2*pi),anglemeas2)

xlabel('frequency')

ylabel('angle k')

legend('calc','meas')

axis([0 30 0 20])
```